Design and Performance of Band-Stop Filters for the TE01 Mode in Circular Waveguide

Kühn, Eberhard
Schwartz, Wolf Dieter

Veröffentlicht in:
Abhandlungen der Braunschweigischen Wissenschaftlichen Gesellschaft Band 25, 1975, S.43-75

Verlag Erich Goltze KG, Göttingen

Design and Performance of Band-Stop Filters for the TE_{01} Mode in Circular Waveguide

by Eberhard Kühn and Wolf Dieter Schwartz*

Communication from the Forschungsinstitut der Deutschen Bundespost, Darmstadt,
and from the Institut für Hochfrequenztechnik der Technischen Universität Braunschweig

Vorgelegt von **Hans Georg Unger**

Abstract

An exact analysis is presented for circular electric TE_{01}° mode band-stop filters with circular and coaxial resonators as proposed by MARCATILI. In order to determine the field in the filter, the structure is subdivided into the three cross-sectional regions: resonator, coupling gap and circular waveguide. In each of these regions the electromagnetic field is represented by complete sets of eigenfunctions. In order to investigate the influence of losses, the resonator field is determined by means of a field-theoretical treatment given by KUROKAWA. A novel mode-matching technique is applied for representing the field in the circular waveguide including the gap region. The unknown expansion coefficients and hence the field distribution are found from the continuity conditions for electromagnetic field across the boundaries between the regions.

From the frequency characteristics of the scattering coefficients the stop frequency and the 3-dB-bandwidth of these filters have been calculated as a function of the dimensions and plotted in design charts. Furthermore, it is shown that two degenerate, higher-order, circular electric TE modes can simultaneously be excited in the coaxial band-stop filter structure leading to a two-pole, maximally-flat frequency response. In addition, a simple design procedure for multi-cavity, single-pole TE_{01}° band-stop filters has been developed.

The theoretical results have been verified by measurements on a two-cavity filter model with coaxial resonators.

* Dr. E. Kühn, c/o Forschungsinstitut der Deutschen Bundespost beim Fernmeldetechnischen Zentralamt, D-61 Darmstadt, Postfach 800

Dipl.-Ing. W. D. Schwartz, c/o Institut für Hochfrequenztechnik, Technische Universität, D-33 Braunschweig, Postfach 3329

Übersicht

Entwurf und Eigenschaften von Bandsperrfiltern für die TE_{01}-Welle im Rundhohlleiter

Von MARCATILI sind axialsymmetrische TE°_{01}-Bandsperrfilter vorgeschlagen worden. Diese Filter werden hier mit einem genauen Berechnungsverfahren untersucht. Dazu wird das Filter in die Querschnittsbereiche Resonator, Koppelspalt und Rundhohlleiter unterteilt, in denen sich das Feld mit einem vollständigen Ansatz von Eigenfunktionen genau beschreiben läßt. Um Verluste zu berücksichtigen, wird das Feld im Resonator mit einem von KUROKAWA angegebenen Verfahren bestimmt. Zur Darstellung des Feldes im Rundhohlleiter einschließlich der Spaltzone ist ein neues Feldentwicklungsprinzip verwendet worden. Die unbekannten Entwicklungskoeffizienten und damit die Feldverteilung ergeben sich aus den Stetigkeitsbedingungen für das elektromagnetische Feld in den Grenzflächen zwischen den Bereichen.

Aus den Frequenzcharakteristiken der Streukoeffizienten sind die Sperrfrequenz und die 3-dB-Bandbreite dieser Filter als Funktion der Abmessungen berechnet und in Entwurfsdiagrammen dargestellt worden. Außerdem wird gezeigt, daß sich durch Anregung zweier entarteter, höherer, axialsymmetrischer TE-Schwingungsformen in der Bandsperre mit koaxialem Resonator eine zweipolige, maximal-flache Frequenzcharakteristik realisieren läßt. Darüber hinaus ist ein einfaches Dimensionierungsverfahren für TE°_{01}-Sperrfilter mit mehreren einkreisigen Resonatoren entwickelt worden.

Die Rechenergebnisse sind durch Messungen an einem Filtermodell mit zwei koaxialen Resonatoren bestätigt worden.

1. Introduction

In millimeter wave transmission systems applying circular waveguides channel diplexers are required for a frequency and mode selective conversion of the TE°_{01} mode of a circular waveguide into the $TE^{\square}_{10}$ mode of a rectangular waveguide. TE°_{01}-$TE^{\square}_{10}$ channel-dropping filters which are appropriate for this application have been investigated in [1] to [5]. These diplexers consist of shunt connected, complementary band-pass and band-stop filters tuned to the center freqency of the channel to be dropped. The mode selective TE°_{01}-$TE^{\square}_{10}$ coupling is done in the band-pass filter. With the aid of the band-stop filter the through circular waveguide is stopped for the channel to be branched.

The aim of this paper is a detailed investigation of the TE°_{01} band-stop filters shown in Fig. 1. Both configurations have been proposed by MARCATILI [1], [2]. Due to the simple geometry and the low losses they are well-suited for the intended purpose. These band-stop filters consist of one or more resonators inserted in the circular waveguide. The incident field is rejected in the vicinity of the common resonant frequency, whereas it is transmitted beyond resonance. Owing to the axial symmetry of the filter structure only circular electric fields are excited by an incident TE°_{01} mode.

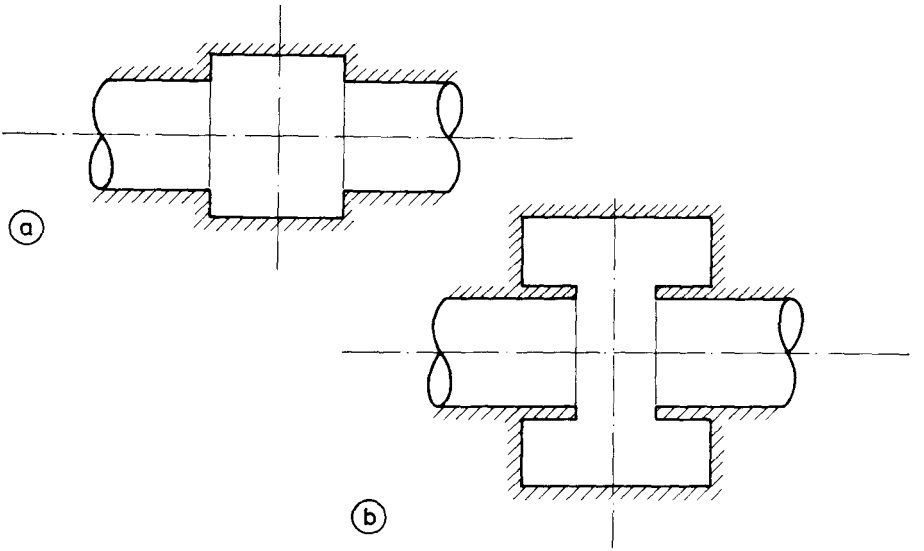

Fig. 1 Cross-sectional view of band-stop filters for the TE_{01}° mode in circular waveguide with
(a) circular cavity,
(b) coaxial cavity.

The waveguide radius has to be chosen such as to prevent the propagation of higher order circular electric modes. Therefore, the useful frequency range is limited by the interval between the cut-off frequencies of the TE_{01}° and TE_{02}° modes, which is slightly below one octave. However, for the following two reasons it is impossible to make full practical use of this band. First, a sufficiently wide guard band has to be provided between the cut-off of the TE_{01}° mode in the circular guide and the stop frequency of the filter. On the other hand, no further resonances of other modes are permitted to occur in the used frequency band. Therefore, in most cases the resonators are excited only in the dominant circular electric mode.

Both filters shown in Fig. 1 allow bandwidths of up to a few percent of the stop frequency to be realized. In the case of broader bandwidths, there is an undue increase in the input reflection in the pass-band. The approximation methods described by MARCATILI allow the considered band-stop filters to be designed with sufficient accuracy only for very narrow bandwidths. Therefore, these filters are analysed in the present paper by means of a generally applicable calculation procedure for the electromagnetic field. In this analysis the influence of losses on the filter performance is taken into account. Data are given for the accurate design of the individual filter structure and for filter cascades as well. Furthermore, a band-stop filter with a coaxial resonator as shown in Fig. 1b is described, which utilizes two degenerate, higher order, circular electric modes instead of the dominant circular electric mode. As a result, a two-pole frequency response is obtained. This filter is especially suited for larger bandwidths.

2. Calculation of the electromagnetic field in the filter

The theoretical treatment of the field problem is based on the filter structure outlined in Fig. 2. This configuration is identical with that shown in Fig. 1b. In order to investigate the properties of the two band-stop filters depicted in Fig. 1 with the model shown in Fig. 2, the calculation of the field has to be carried out taking into account that the maximal width of the gap may be chosen to be as wide as the length of the coaxial resonator.

The following analysis aims at deriving the scattering matrix of the filter. For this purpose it is necessary to express the field inside the coaxial resonator, the coupling gap and the circular waveguide as a function of the cylindrical coordinates (r, φ, z). In the axially symmetrical filter structure only circular electric fields have to be considered if the exciting mode is of the TE°_{01} type. Since it is not possible to represent the field in a closed form, the filter is divided into regions I, II and III according to Fig. 2. In each of these regions the field is completely described by superimposing all eigenfunctions. The tangential electric and magnetic fields across the boundaries between the regions must be continuous because there are neither electric nor magnetic surface currents impressed in these planes. The continuity conditions lead to a sufficient number of coupled linear equations for uniquely determining the unknown expansion coefficients in the field set-up as a function of the excitation parameters.

All metallic surfaces, except the resonator wall, are assumed to have ideal conductivity. This assumption allows an approximation of the losses of the band-stop filter. The dielectric may be characterized by $\varepsilon = \varepsilon_o$ and $\mu = \mu_o$.

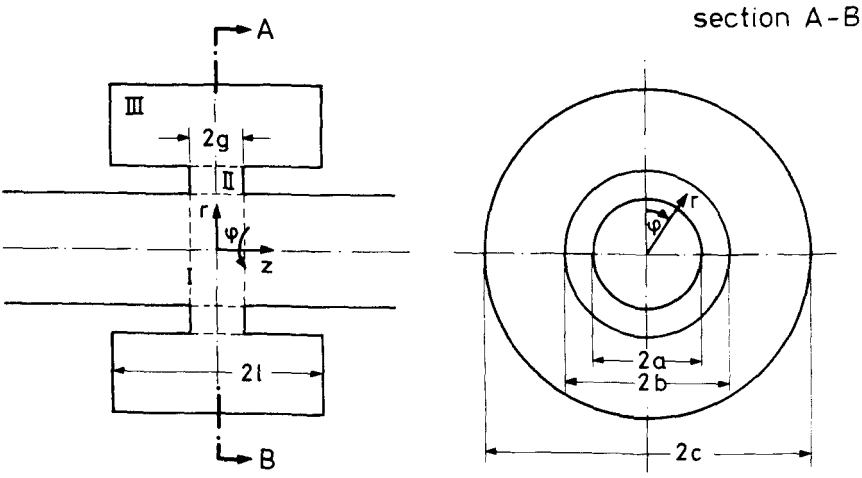

Fig. 2 Coordinate system, dimensions and cross-sectional regions of the analysed TE°_{01} band-stop filter structure.

2.1. The fields in the coupling gap and in the circular waveguide

In the regions I and II the electromagnetic field is suitably derived from wave potentials Ψ representing solutions of the scalar wave equation

$$\Delta\Psi + k^2\Psi = 0 \quad , \qquad k^2 = \omega^2 \mu \varepsilon \, . \tag{1}$$

In eq. (1), k denotes the wave number. According to [6], the field components are calculated from Ψ with the aid of the relations

$$H_z = \frac{1}{j\omega\mu}\left(k^2 + \frac{\partial^2}{\partial z^2}\right)\Psi \qquad E_z = 0$$

$$H_r = \frac{1}{j\omega\mu}\frac{\partial^2\Psi}{\partial r\,\partial z} \qquad E_r = 0 \tag{2}$$

$$H_\varphi = 0 \qquad E_\varphi = \frac{\partial\Psi}{\partial r},$$

where $\frac{\partial}{\partial\varphi} = 0$ has been introduced. In eq. (2), Ψ represents the sum $\sum_i \Psi_i$ over all φ-independant eigenfunctions Ψ_i of gap and waveguide, respectively. Since losses are neglected in both the dielectric and the metallic surfaces in regions I and II, analytically simple solutions of the scalar wave equation can be specified.

Considering that the tangential electric field in the coupling gap vanishes at planes $z = \pm g$ according to the above assumption, the scalar wave potential in region II is given by

$$\Psi^{II} = \sum_{p=1}^{P^{II}} \left(\left(A_p^{II} J_0\left(k_{rs}^{II}(p)\, r\right) + B_p^{II} N_0\left(k_{rs}^{II}(p)\, r\right)\right) \cos\left(k_{zs}^{II}(p)\, z\right) + \right.$$
$$\left. + \left(C_p^{II} J_0\left(k_{ra}^{II}(p)\, r\right) + D_p^{II} N_0\left(k_{ra}^{II}(p)\, r\right)\right) \sin\left(k_{za}^{II}(p)\, z\right)\right). \tag{3}$$

P^{II} denotes the number of circular electric eigenfunctions considered in the radial waveguide II. The axial separation constants in eq. (3) are

$$k_{zs}^{II}(p) = \frac{(2p-1)\pi}{2g}, \tag{4a}$$

$$k_{za}^{II}(p) = \frac{p\pi}{g}. \tag{4b}$$

The indices s and a of the separation constants in eq. (4) indicate that the corresponding distribution of the wave potential is either symmetrical or asymmetrical with respect to $z = 0$. The radial separation constants follow from

$$k^2 = k_{r\langle s\rangle}^{II\,2} + k_{z\langle s\rangle}^{II\,2}. \tag{5}$$

The representation of the radial dependence of Ψ^{II} by Bessel and Neumann functions proves to be mathematically appropriate only as long as $k_{r\langle s\rangle}^{II}(p) \geqq 0$. Under this condition, the solution

$$k_{r\langle s\rangle}^{II}(p) = +\sqrt{k^2 - k_{z\langle s\rangle}^{II\,2}(p)} \qquad k \geq k_{z\langle s\rangle}^{II}(p).$$

has to be taken from eq. (5). In the case of $k_{r\langle\frac{s}{a}\rangle}^{II\,2}(p) < 0$, modified cylindrical functions have to be introduced in eq. (3). Here, the radial separation constants are given by

$$k_{r\langle\frac{s}{a}\rangle}^{II}(p) = -j\,k_{r\langle\frac{s}{a}\rangle}^{II\,\prime}(p) = -j\sqrt{k_{z\langle\frac{s}{a}\rangle}^{II\,2}(p) - k^2} \qquad k < k_{z\langle\frac{s}{a}\rangle}^{II}(p).$$

With the abbreviation $k_r = -j\,k_r'\,(k_r'^2 > 0)$ and the analytic continuation relationships [7] of the cylindrical functions the following conversion formulas can be derived:

$$J_0(k_r r) = I_0(k_r' r),$$

$$N_0(k_r r) = -j\,I_0(k_r' r) - \frac{2}{\pi} K_0(k_r' r).$$

If these expressions were directly introduced in eq. (3), accumulation errors would occur in the numerical calculation since both J_0 and N_0 approach I_0 for large arguments. Therefore, instead of applying the combination of functions (I_0, $\alpha I_0 + \beta K_0$), with constants α and β as given above, (J_0, N_0) in eq. (3) have to be replaced by the pair of functions (I_0, K_0) being linearly independent as well. In order to calculate certain field components Ψ^{II} has to be derived partially with respect to r. This manipulation yields expressions of the form $k_r J_0'(k_r r)$ and $k_r N_0'(k_r r)$. In the case of $k_r^2 < 0$, these terms therefore have to be replaced by $k_r' I_0'(k_r' r)$ and $k_r' K_0'(k_r' r)$, respectively.

Region I includes the gap region and the infinitely long waveguide. Consequently, an integral representation ought to be chosen for the scalar wave potential Ψ^I. This method, however, requires complicated calculations since Fourier-Bessel integrals have to be solved with function-theoretical techniques. In view of this, a simpler field set-up is used here:

The field in the circular waveguide is assumed to be composed of the field of the incident wave defined in the interval $-\infty \leq z \leq +\infty$ and of scattered fields generated at the discontinuity formed by the gap and the resonator. In the regions $z \geq +g$ and $z \leq -g$ the scattered fields consist of TE_{0n}° modes propagating in $+z$ or $-z$ direction, respectively. In order to calculate the scattering field in the region defined by $0 \leq r \leq a$ and $|z| \leq g$, the mode-matching method given in [8] is employed. Following this treatment, the total field is completely represented by three terms:

1. standing circular electric modes of a circular waveguide of radius r = a shorted at $z = +g$,
2. standing circular electric modes of a circular waveguide of radius r = a shorted at $z = -g$ and
3. standing circular electric modes of a radial line enclosed by metallic planes at $z = \pm g$ and including $r = 0$.

The combination of terms 1 and 2 is equivalent to circular electric waveguide modes having a z-dependence of the wave potential according to sine and cosine functions. As soon as the boundary conditions for the electric field in the cross-sectional planes $z = \pm g$ and in the lateral area $r = a$ have been taken into account in the set-up of the scalar wave potential Ψ^I, the following relation holds:

$$\Psi^{I} = \begin{cases} \Psi_0 + \sum_{p=1}^{p^I} (A_p^I \cos(k_z^I(p)\,z) + B_p^I \sin(k_z^I(p)\,z))\, J_0(k_r^I(p)\,r)\, K^I(p)\, e^{-j k_z^I(p)\,g} + \\ \quad + \sum_{p=1}^{p^{II}} \Bigg(\frac{A_p^{II} k_{rs}^{II}(p)\, J_0'(k_{rs}^{II}(p)\,a) + B_p^{II} k_{rs}^{II}(p)\, N_0'(k_{rs}^{II}(p)\,a)}{k_{rs}^{II}(p)\, J_0'(k_{rs}^{II}(p)\,a)} \cdot \\ \qquad \cdot J_0(k_{rs}^{II}(p)\,r) \cos(k_{zs}^{II}(p)\,z) \\ \qquad + \frac{C_p^{II} k_{ra}^{II}(p)\, J_0'(k_{ra}^{II}(p)\,a) + D_p^{II} k_{ra}^{II}(p)\, N_0'(k_{ra}^{II}(p)\,a)}{k_{ra}^{II}(p)\, N_0'(k_{ra}^{II}(p)\,a)} \cdot \\ \qquad \cdot N_0(k_{ra}^{II}(p)\,r) \sin(k_{za}^{II}(p)\,z) \Bigg) & |z| \le g \\ \Psi_0 + \sum_{p=1}^{p^I} (A_p^I \cos(k_z^I(p)\,g) + \operatorname{sign}(z)\, B_p^I \sin(k_z^I(p)\,g)) \cdot \\ \qquad \cdot J_0(k_r^I(p)\,r)\, K^I(p)\, e^{-j k_z^I(p)\,|z|} & |z| \ge g \end{cases} \tag{6a}$$

Ψ_0 contains a TE_{0n}° mode incident from the left-hand side of the waveguide:

$$\Psi_0 = A_n J_0(k_r^I(n)\,r)\, K^I(n)\, e^{-j k_z^I(n)\cdot(z+g)} \qquad n = 1 \text{ or } 2 \text{ or } \ldots P^I. \tag{6b}$$

In eq. (6), P^I denotes the number of TE_{0p}° modes considered in the waveguide. In order to study the influence of evanescent modes on the transmission characteristics of several cascaded band-stop filters, the integer n in eq. (6b) can be chosen arbitrarily. The separation constants result from

$$k_r^I(p) = \frac{x_{0p}'}{a},$$

$$k_z^{I2}(p) = k^2 - k_r^{I2}(p),$$

where x_{0p}' represents the p-th, non-vanishing zero of J_0'. In analogy with k_r^{II} the separation constant k_z^I is given by

$$k_z^I(p) = \begin{cases} + \sqrt{k^2 - k_r^{I2}(p)} & k \ge k_r^I(p) \\ - j\, k_z^{I\prime}(p) = - j \sqrt{k_r^{I2}(p) - k^2} & k \le k_r^I(p). \end{cases}$$

The definition used above is necessary for converting a propagating mode into a mode being aperiodically attenuated in the same direction if the sign of k_z^{I2} becomes negative. With

$$K^I(p) = \frac{\sqrt{\frac{2}{\pi} \frac{k}{k_z^I(p)} \sqrt{\frac{\mu}{\varepsilon}}}}{x_{0p}'\, J_0(x_{0p}')}$$

each waveguide mode is normalized in such a way that its transmitted real power is given by the square of the absolute value of its amplitude.

2.2. The field in the resonator

As in the case of the coupling gap it is possible to represent the scalar wave potential Ψ^{III} in the resonator by superimposing all eigenfunctions of a radial line enclosed by metallic planes at $z = \pm \ell$ and shorted at $r = c$. By this method, however, analytically simple solutions of the eigenfunctions can only be obtained if the metallic resonator wall is assumed to have ideal conductivity. In this paper, the influence of heat losses will be considered. Therefore, the field expansion method described by KUROKAWA [9] will be used in the following for calculating the field in the resonator region. KUROKAWA's treatment is based on the fact that for the application of resonators in filter networks it is not necessary to determine the cavity field accurately, but merely the influence of the resonator on the outer circuitry. Therefore, it is sufficient to expand the continuous fields $\vec{E}^{III}$ and $\vec{H}^{III}$ in the resonator (volume V, surface O, unit vector $\vec{u}$ normal to O) in terms of complete systems of orthogonal eigenfunctions which need not satisfy the boundary conditions, but have to converge towards the actual fields in the quadratic mean. Convergence in this sense means that the integral of the square of the difference between the actual and the approximate fields taken over the cavity volume approaches zero. It can be shown that the complex energy theorem applied to the resonator is valid for the considered systems of eigenfunctions. Therefore, these fields allow the influence of the resonator on the outer circuitry to be described exactly.

The fields are expanded in terms of eigenfunctions representing solutions of the partial differential equations

$$\left.\begin{aligned} \Delta\vec{\Phi}_m + k_\Phi^2\,\vec{\Phi}_m &= 0 \quad \text{in V} \\ \vec{u}\times\vec{\Phi}_m &= 0 \\ \operatorname{div}\vec{\Phi}_m &= 0 \end{aligned}\right\} \text{on O} \tag{7}$$

and

$$\left.\begin{aligned} \Delta\vec{\Theta}_m + k_\Theta^2\,\vec{\Theta}_m &= 0 \quad \text{in V} \\ \vec{u}\cdot\vec{\Theta}_m &= 0 \\ \vec{u}\times\operatorname{curl}\vec{\Theta}_m &= 0 \end{aligned}\right\} \text{on O.} \tag{8}$$

Due to the similar boundary conditions and the resulting improved convergence of the expansion coefficients, it is appropriate to express the electric field in the resonator in terms of the eigenfunctions $\vec{\Phi}_m$ and the magnetic field in terms of the eigenfunctions $\vec{\Theta}_m$. The following three groups of solutions of the differential equations (7) and (8) have to be distinguished:

1. irrotational solutions,
2. solenoidal solutions, and
3. solutions characterized by both vanishing curl and divergence.

According to the nomenclature used in [9], the solutions of $\vec{\Phi}_m$ are denoted by $\vec{E}_a$ and $\vec{F}_\alpha$, whereas $\vec{H}_a$ and $\vec{G}_\lambda$ are the solutions of $\vec{\Theta}_m$. $\vec{E}_a$ and $\vec{H}_a$ constitute the

solenoidal, $\vec{F}_\alpha$ and $\vec{G}_\lambda$ the irrotational contributions. Thus, the fields $\vec{E}^{III}$ and $\vec{H}^{III}$ can be expanded as follows:

$$\vec{E}^{III} \doteq \sum_a \vec{E}_a \iiint_{(V)} \vec{E}^{III} \cdot \vec{E}_a^* \, dV + \sum_\alpha \vec{F}_\alpha \iiint_{(V)} \vec{E}^{III} \cdot \vec{F}_\alpha^* \, dV , \tag{9a}$$

$$\vec{H}^{III} \doteq \sum_a \vec{H}_a \iiint_{(V)} \vec{H}^{III} \cdot \vec{H}_a^* \, dV + \sum_\lambda \vec{G}_\lambda \iiint_{(V)} \vec{H}^{III} \cdot \vec{G}_\lambda^* \, dV \tag{9b}$$

if the orthogonal eigenfunctions are normalized in such a way that

$$\iiint_{(V)} \vec{\Phi}_m \cdot \vec{\Phi}_m^* \, dV = \iiint_{(V)} \vec{\Theta}_m \cdot \vec{\Theta}_m^* \, dV = 1.$$

The asterisk in the preceding equations indicates the complex conjugate of the corresponding quantity. Solutions of $\vec{E}_a$, $\vec{F}_\alpha$, $\vec{H}_a$ and $\vec{G}_\lambda$ will be specified later. Here it may suffice to state that $\vec{u} \times \vec{E}_a$ as well as $\vec{u} \times \vec{F}_\alpha$ vanish on O and thus do not satisfy the boundary conditions for $\vec{u} \times \vec{E}^{III}$ across the aperture in the resonator wall. On the other hand, $\vec{H}_a$ and $\vec{G}_\lambda$ have no normal components on the surface. The modified equal sign $\doteq$ in eq. (9) indicates that the expansions on the right side approximate the actual fields only in quadratic mean.

It has been shown in [4] that the volume integrals in eq. (9) can be transformed into surface integrals by means of simple vector-analytical operations if the resonator is excited only by fields in the aperture of its surface:

$$\iiint_{(V)} \vec{E}^{III} \cdot \vec{E}_a^* \, dV = -j \sqrt{\frac{\mu}{\varepsilon}} \frac{\frac{1}{\omega \mu}}{\frac{1}{Q_a} + j\left(\frac{\omega}{\omega_a'} - \frac{\omega_a'}{\omega}\right)} \iint_{\Delta O} (\vec{E}^{III} \times \vec{u}) \cdot \vec{H}_a^* \, dO , \tag{10a}$$

$$\iiint_{(V)} \vec{E}^{III} \cdot \vec{F}_\alpha^* \, dV = 0 , \tag{10b}$$

$$\iiint_{(V)} \vec{H}^{III} \cdot \vec{H}_a^* \, dV = \frac{\frac{1}{\omega_a \mu}}{\frac{1}{Q_a} + j\left(\frac{\omega}{\omega_a'} - \frac{\omega_a'}{\omega}\right)} \iint_{\Delta O} (\vec{E}^{III} \times \vec{u}) \cdot \vec{H}_a^* \, dO , \tag{10c}$$

$$\iiint_{(V)} \vec{H}^{III} \cdot \vec{G}_\lambda^* \, dV = \frac{1}{j \omega \mu} \iint_{\Delta O} (\vec{E}^{III} \times \vec{u}) \cdot \vec{G}_\lambda^* \, dO. \tag{10d}$$

The integrals on the right-hand side of eqs. (10) have to be extended over the aperture ΔO between gap and resonator. $\vec{u} \times \vec{E}^{III}$ is the actual tangential electric field in this boundary plane. The continuity condition requires $\vec{u} \times \vec{E}^{III} = \vec{u} \times \vec{E}^{II}$. $\vec{E}^{II}$ can be derived from eqs. (2) and (3). In eqs. (10), the abbreviations

$$\frac{1}{Q_a} = \frac{1}{2}\sqrt{\frac{2}{\omega_a \mu \sigma_m}} \iint_{O_m} \vec{H}_a \cdot \vec{H}_a^* \, dO, \tag{11a}$$

$$\omega_a' = \omega_a \left(1 - \frac{1}{2 Q_a}\right) \tag{11b}$$

have been indroduced. Q_a is the internal quality factor of an eigenmode a resulting from the finite conductivity σ_m of the metallic part O_m of the resonator surface. ω_a denotes the angular resonant frequency corresponding to the eigenvalue k_a as defined in eqs. (7) and (8). Due to losses, the effective resonance ω_a' is slightly below ω_a.

Only those of the general solutions $\vec{E}_a$, $\vec{F}_\alpha$, $\vec{H}_a$ and $\vec{G}_\lambda$ obtained for a coaxial cavity are of interest here which lead to circular electric fields. The eigenfunctions $\vec{E}_a$ and $\vec{F}_\alpha$ are not required for the following analysis since merely the magnetic field has to be matched at the boundary between gap and resonator. With unit vectors $\vec{u}_r$, $\vec{u}_\varphi$ and $\vec{u}_z$ defined r-, φ- and z-directions, respectively, the relevant solutions of $\vec{H}_a$ and $\vec{G}_\lambda$ have been given in [4]:

$$\vec{H}_a = \frac{K^{III}(m)}{k^{III}(m,p)} \left(k_r^{III}(m) Z_0'(k_r^{III}(m) r) \begin{Bmatrix} -k_{zs}^{III}(p) \sin(k_{zs}^{III}(p) z) \\ k_{za}^{III}(p) \cos(k_{za}^{III}(p) z) \end{Bmatrix} \vec{u}_r + \right.$$
$$\left. + k_r^{III2}(m) Z_0(k_r^{III}(m) r) \begin{Bmatrix} \cos(k_{zs}^{III}(p) z) \\ \sin(k_{za}^{III}(p) z) \end{Bmatrix} \vec{u}_z \right) \tag{12a}$$
$$m = 1, 2, \ldots M^{III}; \quad p = 1, 2, \ldots P^{III},$$

$$\vec{G}_\lambda^{(1)} = \frac{1}{\sqrt{\pi \ell (b^2 - a^2)}} \begin{Bmatrix} \cos(k_{zs}^{III}(p) z) \\ -\sin(k_{za}^{III}(p) z) \end{Bmatrix} \vec{u}_z \qquad p = 1, 2, \ldots P^{III}, \tag{12b}$$

$$\vec{G}_\lambda^{(2)} = \frac{K^{III}(m) k_r^{III}(m)}{k^{III}(m,p)} \begin{Bmatrix} 1 \\ 1 + \delta_{po} \end{Bmatrix} \left(k_r^{III}(m) Z_0'(k_r^{III}(m) r) \begin{Bmatrix} \sin(k_{zs}^{III}(p) z) \\ \cos(k_{za}^{III}(p) z) \end{Bmatrix} \vec{u}_r + \right.$$
$$\left. + Z_0(k_r^{III}(m) r) \begin{Bmatrix} k_{zs}^{III}(p) \cos(k_{zs}^{III}(p) z) \\ -k_{za}^{III}(p) \sin(k_{za}^{III}(p) z) \end{Bmatrix} \vec{u}_z \right) \tag{12c}$$
$$m = 1, 2, \ldots M^{III}; \quad p = 1, 2, \ldots P^{III}.$$

In eqs. (12) the following abbreviations have been introduced:

$$k_{zs}^{III}(p) = \frac{(2p-1)\pi}{2\ell},$$

$$k_{za}^{III}(p) = \frac{p\pi}{\ell},$$

$$Z_0(k_r^{III}(m) r) = J_0(k_r^{III}(m) r) N_0'(k_r^{III}(m) c) - N_0(k_r^{III}(m) r) J_0'(k_r^{III}(m) c), \tag{13}$$

$k_r^{III}(m)$ is the m-th, non-vanishing root of $Z_0'(k_r^{III}(m) b) = 0$,

$$k^{III2}(m,p) = k_r^{III2}(m) + \begin{Vmatrix} k_{zs}^{III}(p) \\ k_{za}^{III}(p) \end{Vmatrix}^2,$$

$$K^{III}(m) = \frac{1}{\sqrt{\pi \ell \left(\left(\frac{2}{\pi}\right)^2 - (k_r^{III}(m)\, b\, Z_0 (k_r^{III}(m)\, b))^2\right)}},$$

$$\omega^{III}(m, p) = \frac{k^{III}(m, p)}{\sqrt{\mu \varepsilon}}.$$

ω^{III} and k^{III} denote the angular resonant frequency and the eigenvalue of the resonator eigenmodes of types a and λ according to eq. (9), which are specified by the index combination (m, p). M^{III} and P^{III} represent the numbers of standing waves in r- and z-directions, respectively, considered in the field set-up. As in the nomenclature used for the regions I and II, the subscripts s and a characterize the symmetrical and asymmetrical distribution of the longitudinal components $\vec{H}_a$ and $\vec{G}_\lambda$ with respect to $z = 0$. The internal quality factor and the effective resonant frequency are derived from eq. (11):

$$\frac{1}{Q(m, p)} = \pi \sqrt{\frac{2}{\omega^{III}(m, p)\, \mu\, \sigma_m}} \left(\frac{K^{III}(m)}{k^{III}(m, p)}\right)^2 \cdot \left(\left(\frac{2}{\pi}\right)^2 \left(k_{z\langle \overset{s}{a} \rangle}^{III2}(p) + k_r^{III2}(m) \frac{\ell}{c}\right) - (k_r^{III}(m)\, c Z_0 (k_r^{III}(m)\, c))^2 \cdot \left(k_{z\langle \overset{s}{a} \rangle}^{III2}(p) - k_r^{III2}(m) \frac{c - I_{\langle \overset{s}{a} \rangle}^{III}(p)}{a}\right)\right), \tag{14a}$$

$$\omega^{III_r}(m, p) = \omega^{III}(m, p) \left(1 - \frac{1}{2\, Q(m, p)}\right). \tag{14b}$$

The integral $I_{\langle \overset{s}{a} \rangle}^{III}$ in eq. (14a) is given by

$$I_{\langle \overset{s}{a} \rangle}^{III}(p) = \int_{-g}^{+g} \left\langle \begin{matrix} \cos(k_{zs}^{III}(p)\, z) \\ \sin(k_{za}^{III}(p)\, z) \end{matrix} \right\rangle^2 dz = g \left\langle \begin{matrix} + \\ - \end{matrix} \right\rangle \frac{\sin(2\, k_{z\langle \overset{s}{a} \rangle}^{III}(p)\, g)}{2\, k_{z\langle \overset{s}{a} \rangle}^{III}(p)}.$$

2.4. Determination of the expansion coefficients

The requirement of a continuous magnetic field across the boundaries between the regions I, II and III yields a sufficient number of coupled linear equations for uniquely determining the expansion coefficients in the field set-up in terms of the excitation parameters. It is no longer necessary to consider the electric field. According to the set-up chosen, the $\vec{E}$-field is continuous in the cross-sections at $z = \pm g$ and in the lateral area at $r = a$, whereas it is discontinuous across the boundary between gap and resonator. At this boundary, however, the energy relations are satisfied and hence the impedance behaviour of the resonator is exactly described by the field set-up specified for this region if the magnetic field is continuous there.

Matching of the magnetic field at $z = \pm g$ results in the following two equation systems:

$$\frac{1}{2}a^2 k_r^I(m)\, k_z^I(m)\, K^I(m)\, J_0^2(x'_{0m}) \left\langle \begin{matrix} j A_m^I \\ B_m^I \end{matrix} \right\rangle =$$

$$= \sum_{p=1}^{P^{II}} \frac{(-1)^{p+1} k_z^{II}(p)\, I^I(m,p)}{J_0'(k_r^{II}(p)\,a)} \left(J_0'(k_r^{II}(p)\,a) \left\langle \begin{matrix} A_p^{II} \\ C_p^{II} \end{matrix} \right\rangle + N_0'(k_r^{II}(p)\,a) \left\langle \begin{matrix} B_p^{II} \\ D_p^{II} \end{matrix} \right\rangle \right) \qquad (15)$$

$$m = 1, 2, \ldots P^I.$$

In eq. (15) and in the following equations the values taken for the separation constants k_r^{II} and k_z^{II} are those for the symmetrical or asymmetrical case depending on whether the corresponding coeffizients belong to a Ψ^{II}-distribution being even or odd with respect to $z = 0$. The coupling integral $I^I_{\langle {s \atop a} \rangle}$ is given by

$$I^I_{\langle {s \atop a} \rangle}(m,p) = k_{r\langle {s \atop a} \rangle}^{II}(p) \int_0^a J_0'(k_r^I(m)\,r)\, J_0'(k_{r\langle {s \atop a} \rangle}^{II}(p)\,r)\, r\,dr =$$

$$= \begin{cases} \dfrac{x'_{0m} J_0'(x'_{0m})\, k_{r\langle {s \atop a} \rangle}^{II}(p) J_0' k_{r\langle {s \atop a} \rangle}^{II}(p)\,a)}{k_r^{I2}(m) - k_{r\langle {s \atop a} \rangle}^{II2}(p)} & k_r^{I2}(m) \neq k_{r\langle {s \atop a} \rangle}^{II2}(p) \\ \dfrac{1}{2} x'_{0m}\, a\, J_0^2(x'_{0m}) & k_r^{I2}(m) = k_{r\langle {s \atop a} \rangle}^{II2}(p)\,. \end{cases}$$

After inserting the coefficients A^I and B^I from eq. (15) into eq. (6a), Ψ^I only depends on the amplitudes A^{II}, B^{II} and C^{II}, D^{II}. Consequently, the matching of the magnetic field at $r = a$ and $r = b$ yields two equation systems which merely contain the coefficients belonging to the symmetrical or asymmetrical field distribution of region II as a function of the amplitude of the incident TE°_{0n} mode. The magnetic field is continuous at $r = a$ if the following conditions hold:

$$\sum_{q=1}^{P^{II}} \left\{ \frac{2}{a} k_z^{II}(q) \cdot (-1)^q \sum_{n=1}^{P^I} \frac{k_r^{I2}(n)}{k_z^I(n)\, x'_{0n} J_0(x'_{0n})} I^I(n,q)\, I_1^{II}(m,n) \left\langle \begin{matrix} A_q^{II} \\ C_q^{II} \end{matrix} \right\rangle + \right.$$

$$+ \left(-\delta_{qm} \left\langle \begin{matrix} j \\ 1 \end{matrix} \right\rangle \frac{k_r^{II2}(q)\, g\, W(k_r^{II}(q)\,a)}{k_r^{II}(q) J_0'(k_r^{II}(q)\,a)} + \frac{2}{a} k_z^{II}(q) \cdot (-1)^q \frac{N_0'(k_r^{II}(q)\,a)}{J_0'(k_r^{II}(q)\,a)} \cdot \right.$$

$$\left. \left. \cdot \sum_{n=1}^{P^I} \frac{k_r^{I2}(n)}{k_z^I(n)\, x'_{0n} J_0(x'_{0n})} I^I(n,q)\, I_1^{II}(m,n) \right) \left\langle \begin{matrix} B_q^{II} \\ D_q^{II} \end{matrix} \right\rangle \right\} = \qquad (16)$$

$$= \langle \pm \rangle\, j k_r^{I2}(p) J_0(x'_{0p}) K^I(p) I_1^{II}(m,p) A_p$$

$$m = 1, 2, \ldots P^{II}; \quad p = 1 \text{ or } 2 \text{ or } \ldots P^I.$$

The coupling integral I_1^{II} is defined by

$$I_1^{II}(m,p) = e^{-j k_z^I(p) g} \int_{-g}^{+g} \left\langle \begin{matrix} \cos(k_z^I(p)\,z) \cos(k_{zs}^{II}(m)\,z) \\ \sin(k_z^I(p)\,z) \sin(k_{za}^{II}(m)\,z) \end{matrix} \right\rangle dz =$$

$$= \begin{cases} \left\langle \begin{matrix} +1 \\ -j \end{matrix} \right\rangle \dfrac{k_{z\langle {s \atop a} \rangle}^{II}(m)}{k_z^{I2}(p) - k_{z\langle {s \atop a} \rangle}^{II2}(m)} (-1)^m (1 \langle \pm \rangle e^{-2 j k_z^I(p) g}) k_z^{I2}(p) \neq k_{z\langle {s \atop a} \rangle}^{II2}(m) \\ g e^{-j k_z^I(p) g} \qquad\qquad k_z^{I2}(p) = k_{z\langle {s \atop a} \rangle}^{II2}(m). \end{cases}$$

W in eq. (16) represents the modified Wronskian determinant

$$W(k_r a) = k_r (J_0(k_r a) N_0'(k_r a) - J_0'(k_r a) N_0(k_r a)) = \begin{cases} \dfrac{2}{\pi a} & k_r^2 \geq 0 \\ -\dfrac{1}{a} & k_r^2 < 0. \end{cases}$$

Matching of the magnetic field across r = b leads to the relations

$$\sum_{p=1}^{P^{II}} \left((\delta_{pq}\, g\, k_r^{II2}(p) J_0(k_r^{II}(p) b) - V(q,p) k_r^{II}(p) J_0'(k_r^{II}(p) b)) \begin{pmatrix} A_p^{II} \\ C_p^{II} \end{pmatrix} + \right.$$
$$\left. + (\delta_{pq}\, g\, k_r^{II2}(p) N_0(k_r^{II}(p) b) - V(q,p) k_r^{II}(p) N_0'(k_r^{II}(p) b)) \begin{pmatrix} B_p^{II} \\ D_p^{II} \end{pmatrix} \right) = 0 \qquad (17)$$
$$q = 1, 2, \ldots P^{II}$$

where

$$V(q,p) = \sum_{\bar{p}=1}^{P^{III}} 2\pi b\, I_2^{II}(q,\bar{p}) I_2^{II}(p,\bar{p}) \left(\frac{1}{\pi \ell (c^2 - b^2)} + \right.$$
$$+ \sum_{\bar{m}=1}^{M^{III}} \left(\frac{K^{III}(\bar{m})}{k^{III}(\bar{m},\bar{p})} k_r^{III2}(\bar{m}) Z_0(k_r^{III}(\bar{m}) c) \right)^2 \cdot$$
$$\left. \cdot \left(\frac{j \dfrac{\omega}{\omega(\bar{m},\bar{p})}}{\dfrac{1}{Q(\bar{m},\bar{p})} + j \left(\dfrac{\omega}{\omega^{III'}(\bar{m},\bar{p})} - \dfrac{\omega^{III'}(\bar{m},\bar{p})}{\omega} \right)} + \frac{k_z^{III2}(\bar{p})}{k_r^{III2}(\bar{m})} \right) \right)$$

and

$$I_{2\langle{}^{s}_{a}\rangle}^{II}(q,p) = \int_{-g}^{+g} \begin{pmatrix} \cos(k_{zs}^{II}(q) z) \cos(k_{zs}^{III}(p) z) \\ \sin(k_{za}^{II}(q) z) \sin(k_{za}^{III}(p) z) \end{pmatrix} dz =$$
$$= \begin{cases} -2(-1)^q \dfrac{k_{z\langle{}^{s}_{a}\rangle}^{II}(q)}{k_{z\langle{}^{s}_{a}\rangle}^{II2}(q) - k_{z\langle{}^{s}_{a}\rangle}^{III2}(p)} \begin{pmatrix} \cos(k_{zs}^{III}(p) g) \\ \sin(k_{za}^{III}(p) g) \end{pmatrix} & k_{z\langle{}^{s}_{a}\rangle}^{II}(q) \neq k_{z\langle{}^{s}_{a}\rangle}^{III}(p) \\ g & k_{z\langle{}^{s}_{a}\rangle}^{II}(q) = k_{z\langle{}^{s}_{a}\rangle}^{III}(p). \end{cases}$$

The equation systems (16) and (17) allow the coefficients A^{II}, B^{II} and C^{II}, D^{II} to be determined depending on the amplitude A_p of the incident TE_{0p}° mode. This can be done, for instance, with the aid of the Gaussian algorithm.

3. The scattering matrix of the filter

The elements of the scattering matrix of the filter in Fig. 2 are defined by the quotient of the amplitudes of the reflected or transmitted and the incident mode. Consequently, for the reference planes $z = \pm g$ the following relations hold:

$$\begin{Bmatrix} S_{11}(m,n) \\ S_{21}(m,n) \end{Bmatrix} = \frac{j}{a\, k_z^I(m)\, K^I(m)\, x'_{0m}\, J_0^2(x'_{0m})} \cdot$$
$$\cdot \Bigg((1 + e^{-2j k_z^I(m) g}) \sum_{p=1}^{P^{II}} \frac{(-1)^p k_{zs}^{II}(p)\, I_s^I(m,p)}{J_0'(k_{rs}^{II}(p)\, a)} \cdot$$
$$\cdot \Big(J_0'(k_{rs}^{II}(p)\, a) \frac{A_p^{II}}{A_n} + N_0'(k_{rs}^{II}(p)\, a) \frac{B_p^{II}}{A_n} \Big) \qquad (18)$$
$$\{\mp\} (1 - e^{-2j k_z^I(m) g}) \sum_{p=1}^{P^{II}} \frac{(-1)^p k_{za}^{II}(p)\, I_a^I(m,p)}{J_0'(k_{ra}^{II}(p)\, a)} \cdot$$
$$\cdot \Big(J_0'(k_{ra}^{II}(p)\, a) \frac{C_p^{II}}{A_n} + N_0'(k_{ra}^{II}(p)\, a) \frac{D_p^{II}}{A_n} \Big) \Bigg)$$
$$+ \begin{Bmatrix} 0 \\ \delta_{mn} e^{-2j k_z^I(n) g} \end{Bmatrix} \qquad m, n = 1, 2, \ldots P^I.$$

The subscript m in eq. (18) characterizes the TE°_{0m} modes excited at ports 1 ($z = -g$) and 2 ($z = +g$). The subscript n refers to the TE°_{0n} mode incident at port 1. The reciprocity of the filter requires $S_{12}(m,n) = S_{21}(n,m)$. Furthermore, $S_{22}(m,n) = S_{11}(m,n)$ applies since the configuration is symmetrical and both reference planes have the same distance from $z = 0$.

4. Calculation of a simplified equivalent network

For deriving the characteristic parameters of the band-stop filter shown in Fig. 2 it is only necessary to consider the scattering coefficients of the TE°_{01} mode. The stop frequency f_0 and the 3-dB-bandwidth Δf can be obtained from the relationships $|S_{21}(1,1)| = |S_{21}(1,1)|_{min}$ and $|S_{11}(1,1)| = |S_{11}(1,1)|_{max}/\sqrt{2}$. In the loss-free case ($\sigma_m \to \infty$) the conditions $|S_{21}(1,1)|_{min} = 0$ and $|S_{11}(1,1)|_{max} = 1$ are satisfied at resonance. The quotient of f_0 and Δf represents the quality factor of the resonant circuit loaded by the characteristic impedances of the waveguides connected at both filter ports:

$$Q_L = \frac{f_0}{\Delta f}. \qquad (19)$$

The resonant circuit is loaded by both internal and external losses which can be described by quality factors denoted by Q_{int} and Q_{ext}:

$$\frac{1}{Q_L} = \frac{1}{Q_{int}} + \frac{1}{Q_{ext}}. \qquad (20)$$

For $\sigma_m \to \infty$ $Q_L = Q_{ext}$ holds. Following these formulas, the internal quality factor can be found by comparing the loaded Q factors obtained by considering and neglecting the internal losses, respectively. In this case the relation $Q_{int} \gg Q_{ext}$ applies to all bandwidths of practical interest, i.e. $|S_{11}(1,1)|_{max} \approx 1$ and $|S_{21}(1,1)|_{min} \approx 0$.

For the investigated band-stop filters the phase angle of the input reflection coefficient $S_{11}(1,1) \cdot \exp(j 4\pi g/\lambda_g)$ at the reference plane $z = 0$ is approximately 180°

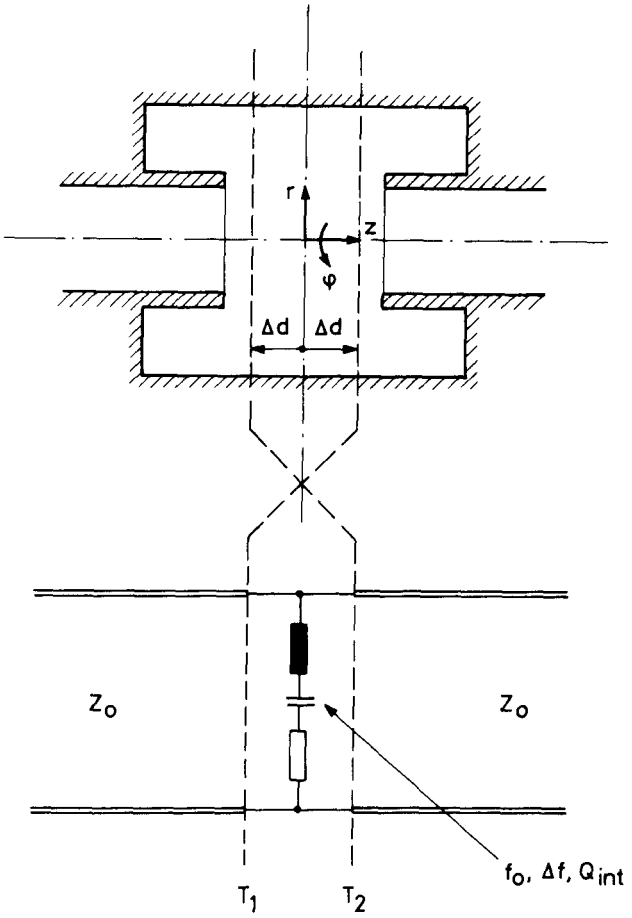

Fig. 3 Equivalent network of a single-pole TE_{01}° band-stop filter valid in the frequency range close to the fundamental circular electric resonance of the cavity.

at resonance (λ_g is the guide-wavelength of the TE_{01}° mode). Hence, the resonator can be represented in an equivalent network by a series resonant circuit having the same resonant frequency, 3-dB-bandwidth and losses (Fig. 3). It must be mentioned in this context, that this model allows a satisfactorily accurate description of the electrical performance of the filter only in a narrow frequency range close to f_0 since a broadband approximation of a circuit consisting of distributed elements requires an infinite number of elements. The connecting points of the series resonant circuit are separated from the symmetry plane of the filter by

$$\Delta d = \frac{\lambda_{g_0}}{4} \cdot \frac{\pi - \arg\left(S_{11}(1,1)\right) \mid_{f_0}}{\pi} - g \tag{21}$$

if $S_{11}(1,1)$ is taken from eq. (18). Depending on whether the phase angle of the reflection coefficient at $z = 0$ is inductive or capacitive, the resonant circuit shorts the line in a plane behind or in front of the filter center as seen from the point of incidence.

5. Cascading of band-stop filters

Cascading of band-stop filters provides a frequency response having both a flattened pass-band and stop-band as well as steeper skirts. It is obvious that better selectivity is obtained at the price of higher losses.

5.1 Design of multi-cavity band-stop filters

For the design of multi-cavity filters it is appropriate to start from an equivalent network having the desired electrical properties and to realize, by way of approximation, the corresponding microwave circuit by substituting step by step the equivalent distributed elements for the known lumped elements [10]. This approach is applicable here because filters having narrow bandwidths of only a few percent are considered. The numerical results demonstrate that the investigated band-stop filters have extremely low loss and therefore losses are neglected in the design procedure described below.

The design method is based on the N element low-pass prototype filter shown in Fig. 4a. If f' denotes the operating frequency in this prototype network ($-\infty \leq f' \leq +\infty$) and f_1' the cut-off where the reflected and transmitted powers are equal, the pass-band and stop-band of this low-pass are characterized by the relations $|f'| \leq |f_1'|$ and $|f'| \geq |f_1'|$, respectively. The normalized elements g_i in Fig. 4a can be expressed by the actual inductances L_i' and capacitances C_i' as follows:

$$g_i = \begin{cases} c_i' = 2\pi f_1' \cdot C_i' \cdot Z_0 & i = 1, 3, 5 \ldots \\ l_i' = 2\pi f_1' \cdot L_i'/Z_0 & i = 2, 4, 6 \ldots \end{cases} \tag{22}$$

The distribution of the parameters g_i in terms of i determines the frequency response of the low-pass. These normalized quantities for prototype filters having either a transfer characteristic of BUTTERWORTH or CHEBYSHEV type or a maximally-flat group-delay characteristic are listed in [10]. In the case of the BUTTERWORTH filter, g_i is described by the simple analytical expression

$$g_i = 2 \sin\left(\frac{2i-1}{2N}\pi\right) \qquad i = 1, 2, \ldots N. \tag{23}$$

This type of filter represents a compromise between the contradicting requirements for both high selectivity and low signal distortion.

With the aid of the frequency transformation

$$\frac{f'}{f_1'} = \frac{1}{Q_L\left(\frac{f}{f_0} - \frac{f_0}{f}\right)} \tag{24}$$

it is possible to transform the low-pass filter into a band-stop filter in the actual frequency range $0 \leq f \leq \infty$. The center frequency of the band-stop filter is located at f_0, the bandwidth is given by

$$\Delta f = \frac{f_0}{Q_L}. \tag{25}$$

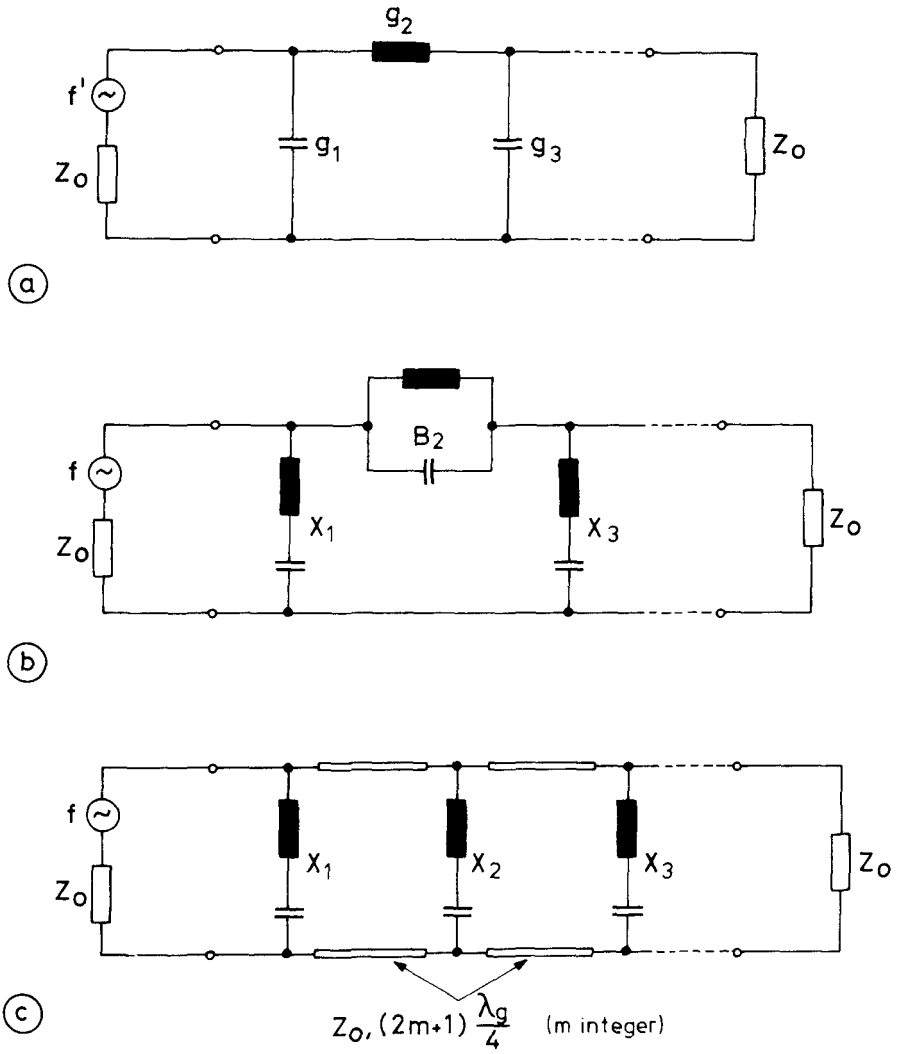

Fig. 4 Design procedure for cascaded single-pole TE_{01}° band-stop filters
(a) lumped-element, low-pass prototype filter,
(b) lumped-element band-stop filter derived from (a) by means of the frequency transformation (24),
(c) equivalent network of the band-stop filter in (b) consisting exclusively of series resonant circuits and additional $\lambda_g/4$-transformers.

Hence, Q_L in eq. (24) constitutes the quality factor of the filter loaded by the characteristic impedances Z_0 of the lines connected on both sides. Fig. 4b shows the result of the frequency transformation (24). The capacitances C_i' lead to the series resonant circuits with the reactances $X_1, X_3, X_5 \ldots$, whereas the inductances L_i' lead to the parallel resonant circuits with the susceptances $B_2, B_4, B_6 \ldots$ The band-stop filters described in this paper allow only series resonant circuits shunting the line to be realized. Therefore, it is necessary to replace the parallel resonant circuits in Fig. 4b by equivalent series resonant circuits provided with additional line sections of length $(2m + 1)\,\lambda_g/4$ where $m = 0, 1, 2 \ldots$ (Fig. 4c). These frequency-independent $\lambda_g/4$-transformers are not feasible in practice. A useful approximation is obtained by choosing the line lengths to be $(2m + 1)\,\lambda_{g_0}/4$, so that an optimum agreement occurs at resonance. The reactances in Fig. 4c are given by

$$X_i = \frac{Q_L Z_0}{g_i}\left(\frac{f}{f_0} - \frac{f_0}{f}\right) \qquad i = 1, 2, \ldots N. \tag{26}$$

According to eq. (26), the external Q-factor of each of these resonant circuits being tuned to f_0 and loaded by impedances Z_0 on both sides is

$$Q_{ext\,i} = \frac{2\,Q_L}{g_i} \qquad i = 1, 2, \ldots N. \tag{27}$$

For the 3-dB-bandwidth of the single circuits, eq. (27) yields

$$\Delta f_i = \frac{f_0}{Q_{ext\,i}} = \frac{g_i}{2}\,\Delta f \qquad i = 1, 2, \ldots N. \tag{28}$$

For given values of f_0, Δf and N as well as for a prescribed type of frequency characteristic the filter cascade is designed as follows:

1. The normalized circuit parameters g_i are either derived directly from eq. (23) or taken from the tables given in [10], depending on N and the desired type of frequency characteristic.
2. The bandwidth Δf_i of each resonant circuit is calculated by means of eq. (28). With f_0 and Δf_i the resonator dimensions can be determined from the design charts (Figs. 7 to 9) which will be described in detail in the next chapter.
3. The requirement that the short-circuit planes of adjacent series resonant circuits in Fig. 4c be located at intervals of $(2m + 1)\,\lambda_{g_0}/4$ allows the distance between the symmetry planes of the filters to be determined with the aid of the quantity Δd which can also be taken from the design charts. To reduce the unwanted frequency dependence of the connecting lines, m should be chosen as small as possible. A lower limit of the filter separation is prescribed either by the filter construction or by the fact that no interaction is allowed to occur between neighbouring cavities via evanescent higher-order TE°_{0n} modes. Depending on the difference between the cut-off of the TE°_{02} mode in the waveguide and the stop frequency of the filter, m assumes an integer value of 1, 2 or 3.

5.2. Calculation of the frequency characteristics

The well-known procedure of determining the scattering matrix of a filter cascade by means of the transmission matrix [6] is numerically applicable only if all evanescent modes in the connecting lines are disregarded. This neglection is not permissible if, for instance, the problem to investigate is whether the chosen number $(2\,m + 1)$ of quarter-wavelengths between adjacent filters is large enough for eliminating the influence of higher-order modes. In this case, the overall scattering matrix has to be derived directly from the corresponding matrices of the individual filters. According to [4], the resulting matrix [S] of a two-filter assembly with scattering matrices denoted by [S'] and [S''] (Fig. 5) is given by

$$\begin{aligned}
[S_{11}] &= [S'_{11}] + [S'_{12}]\,[S''_{11}]\,[M]^{-1}\,[S'_{21}],\\
[S_{12}] &= [S_{21}] = [S''_{21}]\,[M]^{-1}\,[S'_{21}],\\
[S_{22}] &= [S''_{22}] + [S''_{21}]\,[M]^{-1}\,[S'_{22}]\,[S''_{12}]
\end{aligned} \tag{29}$$

where

$$[M] = [1] - [S'_{22}]\,[S''_{11}].$$

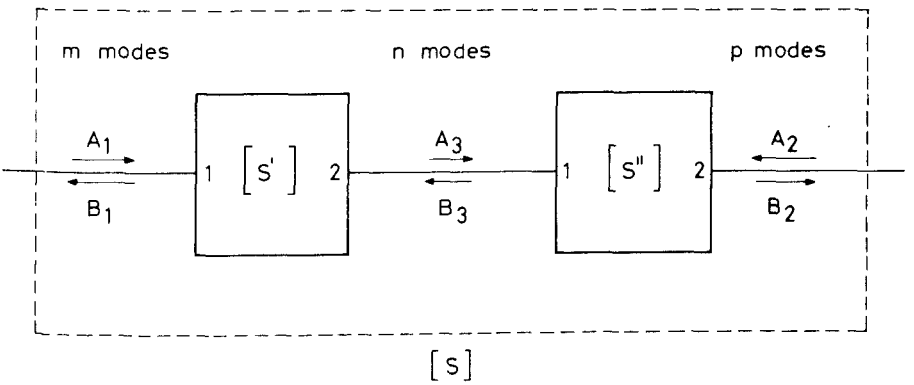

Fig. 5 Circuit configuration for deriving the scattering matrix of cascaded filter networks.

In the case of filter cascades consisting of more than two elements, this procedure has to be applied repeatedly since a general formation law does not exist. The elements of the individual scattering matrices are described by eq. (18) with a shift of the reference planes being taken into account. With the denotations used in Fig. 6, the scattering parameters in the shifted planes can be expressed by

$$\begin{aligned}
\bar{S}_{11}(m,n) &= S_{11}(m,n)\cdot e^{-j\,(k_z^I(m)+k_z^I(n))\,d_1},\\
\bar{S}_{12}(m,n) &= \bar{S}_{21}(n,m) = S_{21}(n,m)\cdot e^{-j\,(k_z^I(m)\,d_1 + k_z^I(n)\,d_2)},\\
\bar{S}_{22}(m,n) &= S_{11}(m,n)\cdot e^{-j\,(k_z^I(m)+k_z^I(n))\,d_2}.
\end{aligned} \tag{30}$$

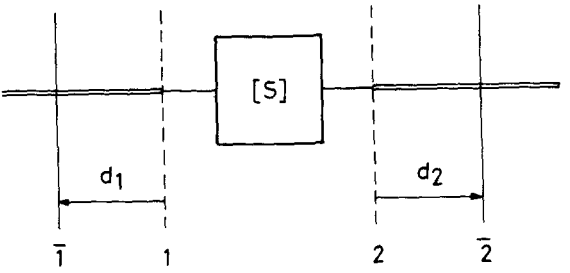

Fig. 6 Circuit configuration for deriving the variation of the scattering parameters by shifting the reference planes.

6. Numerical results

The numerical calculations have been carried out with a computer program written in FORTRAN IV. For arbitrarily chosen dimensions, the program allows to determine the characteristic equivalent network parameters of a single resonator as well as the frequency dependence of the scattering coefficients of an individual or several cascaded filters.

Table 1

Accuracy of the electromagnetic field set-up demonstrated by the relationships between stop frequency f_0 (fundamental circular electric resonance), 3-dB-bandwith Δf, TE°_{01} input reflection coefficient S_{11} (1,1) taken at $z = 0$ and at f_0, TE°_{01} transmission coefficient S_{21} (1,1) taken at $z = 0$ and at f_0 and the summation superscripts P^{I}, P^{II}, P^{III} and M^{III} considered in the analysis of a TE°_{01} band-stop filter designed for the following data: $a = 8.5$ mm, $b = 9.5$ mm, $c = 14.5$ mm, $g = 2.0$ mm, $\ell = 3.0$ mm, $\sigma_m = \infty/14 \cdot 10^6$ $(\Omega m)^{-1}$ (dc conductivity of brass)

$P^{I} = P^{II} = P^{III} = M^{III}$	f_0 in GHz	Δf in MHz	S_{11} (1,1) $\mid_{z=0}$*	S_{21} (1,1) $\mid_{z=0}$*
1	34.749/34.747	347.91/347.80	1.,178.40/0.986,178.40	0./0.014,–1.59
2	34.255/34.253	476.11/475.95	1.,178.27/0.992,178.27	0./0.008,–1.72
3	34.128/34.126	514.27/514.11	1.,178.21/0.993,178.21	0./0.007,–1.78
4	34.054/34.052	532.92/532.76	1.,178.18/0.993,178.18	0./0.007,–1.81
5	34.028/34.026	541.47/541.31	1.,178.16/0.993,178.16	0./0.007,–1.84
6	34.014/34.012	546.81/546.64	1.,178.14/0.994,178.14	0./0.007,–1.85
7	34.000/33.999	550.59/550.42	1.,178.13/0.994,178.13	0./0.006,–1.88
8	33.995/33.993	552.78/552.60	1.,178.12/0.994,178.12	0./0.006,–1.88
9	33.992/33.990	554.35/554.18	1.,178.11/0.994,178.11	0./0.006,–1.89
10	33.988/33.986	555.65/555.48	1.,178.10/0.994,178.10	0./0.006,–1.89

* The scattering parameters are listed in the following form: absolute value, argument in degrees.

6.1. Accuracy of the mathematical procedure

The number of eigenfunctions considered in the field set-up for each region determines the accuracy of the numerical results. An exact solution is obtained only if the sums have an infinite number of elements. Table 1 shows the convergence of stop frequency, bandwidth and scattering parameters as a function of the number of terms. In this case, a band-stop filter with a coaxial resonator having typical dimensions is analysed. Merely a few elements are needed for an accurate calculation of the filter performance. Furthermore, it can be seen that the losses are low enough to be neglected for establishing the design charts described in the following section. This approximation holds if the band-stop filters have fractional bandwiths of practical interest and if the metallic boundaries have high conductivity and low surface roughness.

6.2. Design charts

Figs. 7 to 9 summarize design data for three different types of band-stop filters. The calculations are carried out for a circular waveguide of 8.5 mm inner radius. If the only propagating circular electric mode is the TE_{01}° mode, the covered frequency range corresponds to the R-band (26.4 – 40.1 GHz). The properties of filters having different waveguide radii can be found by applying scaling techniques. If the geometry differs by a factor of $\bar{a}/a$, where $\bar{a}$ represents the new radius, the following conversion formulas are valid:

$$\begin{aligned} &\bar{f}_0 = a/\bar{a} \cdot f_0; \qquad \Delta\bar{f} = a/\bar{a} \cdot \Delta f; \qquad \Delta\bar{d} \approx \bar{a}/a \cdot \Delta d; \\ &\bar{Q}_{ext} = Q_{ext}; \qquad \bar{Q}_{int} = \sqrt{\bar{a}/a}\, Q_{int}. \end{aligned} \tag{31}$$

The characteristic parameters f_0, Δf and Δd of a TE_{01}° band-stop filter utilizing the dominant circular electric resonance of a circular cavity as shown in Fig. 1 a are plotted in Fig. 7. The field configuration corresponds approximately to the TE_{021}° mode of the equivalent, but entirely closed cavity [1]. In order to allow this mode to be excited in the considered frequency range, the cavity diameter has to be increased with respect to the waveguide diameter in order to enable the TE_{02}° mode to propagate. A design procedure has been described in [1] which is applicable only for very small bandwidths. TANGA (in [3]) has experimentally determined f_0 and Δf for filters having broader stop-bands. The numerical results plotted in Fig. 7a are in good agreement with these measured data. For the design of filter cascades the position of the effective short-circuit planes at resonance must be known. Fig. 7b demonstrates that, in contrast to the analysis given in [1], these planes do not coincide with the symmetry plane of the filter.

Moreover, it can be seen from Fig. 7a that the obtainable bandwidth increases with the cavity radius. An upper limit for the 3-dB-bandwidth is given by the unwanted input reflection in the pass-band increasing with Δf. For a prescribed waveguide size broader stop-bands are therefore achievable only in a relatively narrow frequency range. By appropriately selecting the waveguide radius it is possible, however, to

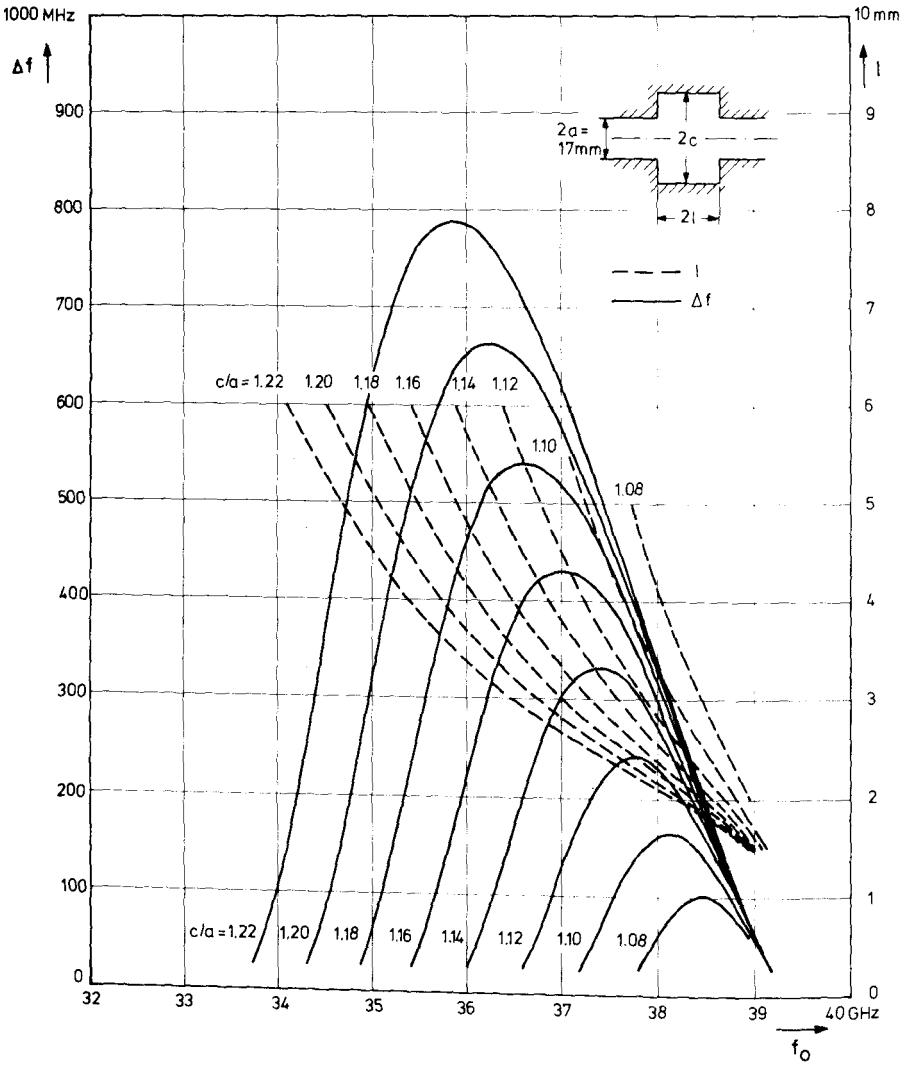

Fig. 7 Design charts for a single-pole TE°_{01} band-stop filter with circular cavity (modified TE°_{021} resonance)
(a) cavity dimensions,

realize broader stop-bands in a wider frequency range. But then, cascading of several filters with specified electrical characteristics requires additional tapers in general.

Band-stop filters with a coaxial cavity as in Fig. 1b are better suited for the intended application. Design charts for three different resonator lengths are presented in Fig. 8. The dimensions are chosen to allow the fundamental circular electric mode to resonate in the considered frequency range. Hence, the field distribution is similar

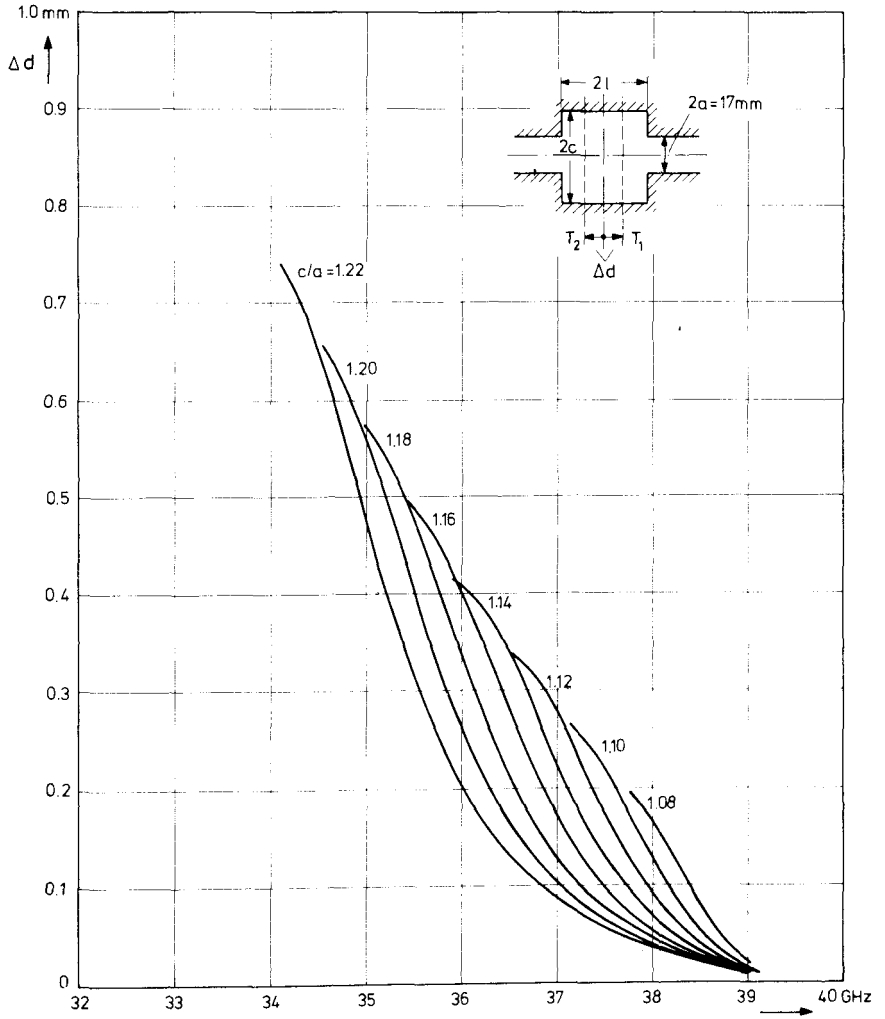

Fig. 7 (b) position of the short-circuit planes at resonance.

to the TE_{011}° mode of the corresponding structure being completely shorted at r = b. These band-stop filters have also been proposed by MARCATILI [2]. His design procedure is based on the assumption that the width of the gap is small compared to λ_{g_0}. The numerical results indicate that this approach only holds for very narrow bandwidths. The charts in Fig. 8 satisfactorily cover the interesting range of f_0 and Δf for the designed purpose. Quality factors of $Q_{ext} < 25$ cannot be realized with these filters if the pass-band reflection is to be kept low. This is why the solution providing the smallest gap has to be chosen if various filter dimensions leading to the same electrical performance are offered by the charts in Fig. 8. In addition, the computations revealed that the distance Δd between the center of the filter and its short-circuit planes at resonance is negligible in all practical cases.

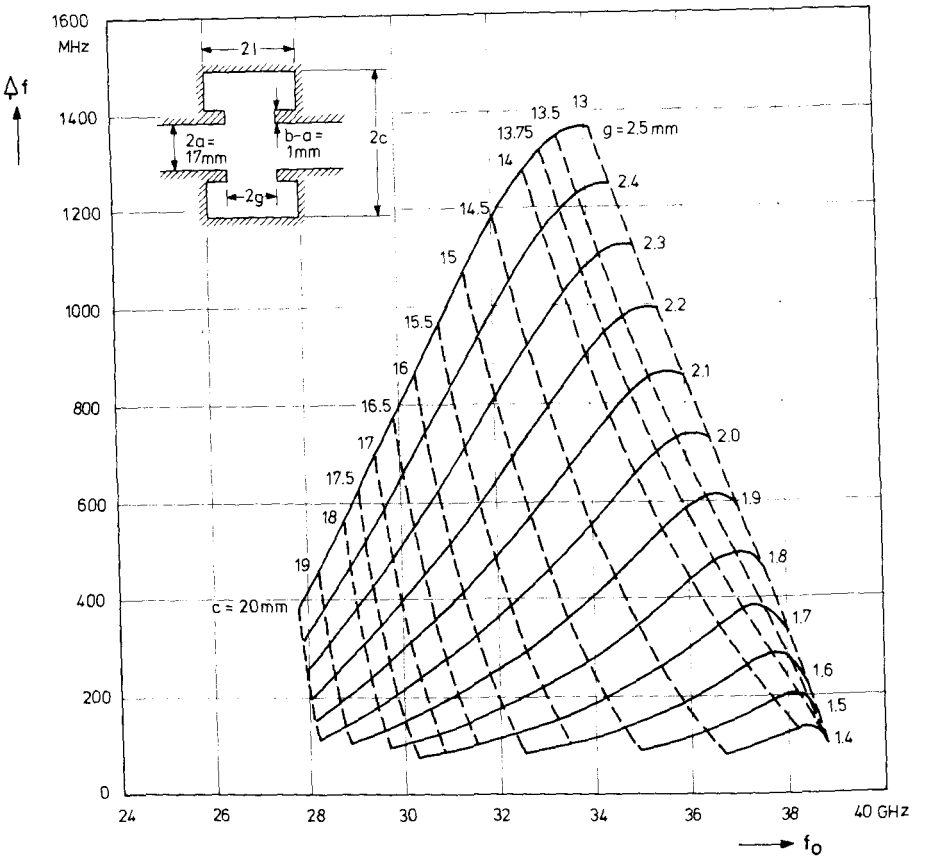

Fig. 8 Design charts for a single-pole TE°_{01} band-stop filter with coaxial cavity (modified TE°_{011} resonance)
(a) $\ell = 3.0$ mm,

It has been mentioned in the introduction that it is possible to realize a two-pole frequency response by suitably designing the coaxial resonator of the filter sketched in Fig. 1b. In this case, a degenerate, circular electric mode is excited. The field of this mode represents a superposition of the TE°_{012} and TE°_{013} modes modified by fringing fields in the gap region. This coupling mechanism can be explained as follows. The gap cut into the center conductor causes a decrease in the resonant frequencies of all TE°_{01n} modes since the tangential electric field does not completely vanish across r = b thus simulating a reduced inner radius of the cavity. Consequently, the resonant frequency is lowered the more, the tighter the coupling between waveguide and resonator. Modes characterized by an odd subscript n have a symmetrical distribution of the tangential field components across the gap and hence the coupling is strong. On the other hand, weak coupling occurs if the number n of standing waves inside the

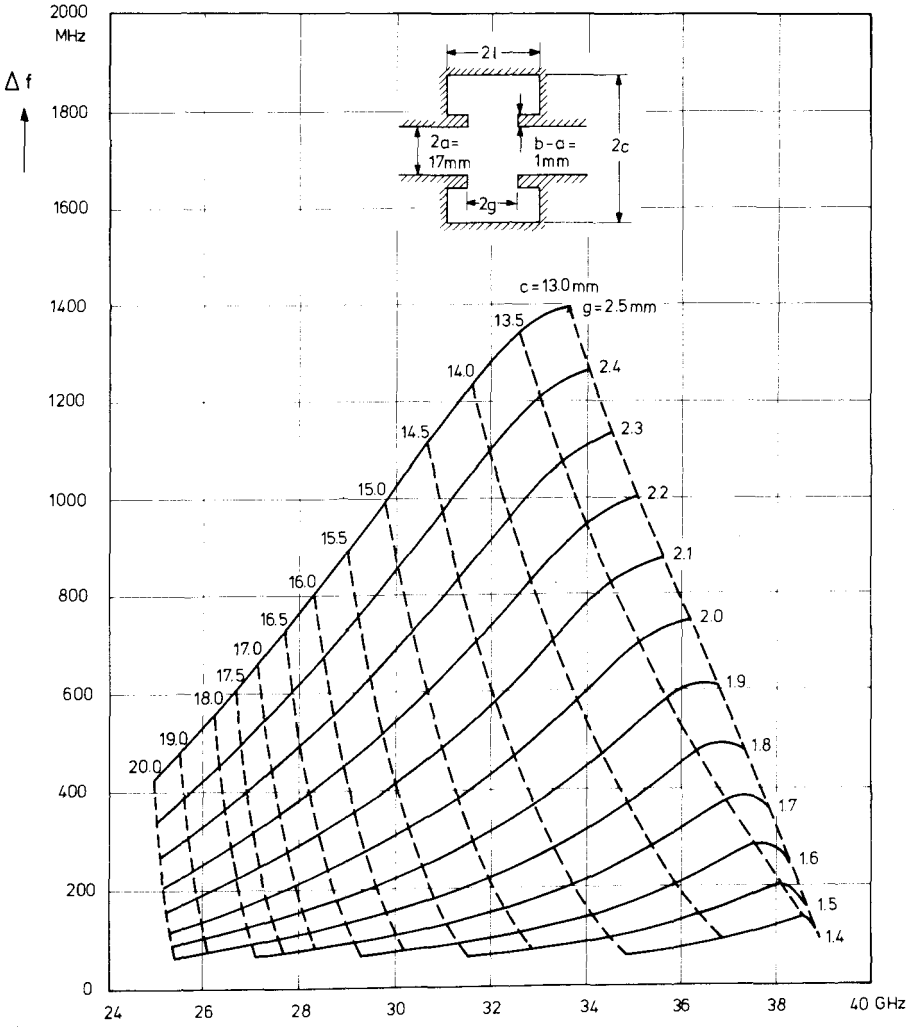

Fig. 8 (b) $\ell = 3.5$ mm,

cavity is even. By a suitable increase of the longitudinal filter dimensions the modified TE_{012}° and TE_{013}° fields can actually be coupled at a common resonant frequency. This two-pole, maximally-flat band-stop filter is applicable if it is possible to achieve a sufficiently large interval between the stop frequencies of the first (TE_{011}°) and this second degenerate resonance. Furthermore, the radial cavity dimensions have to be selected such as to keep the TE_{021}° and higher-order circular electric modes below resonance in the considered frequency range. The numerical results demonstrate that

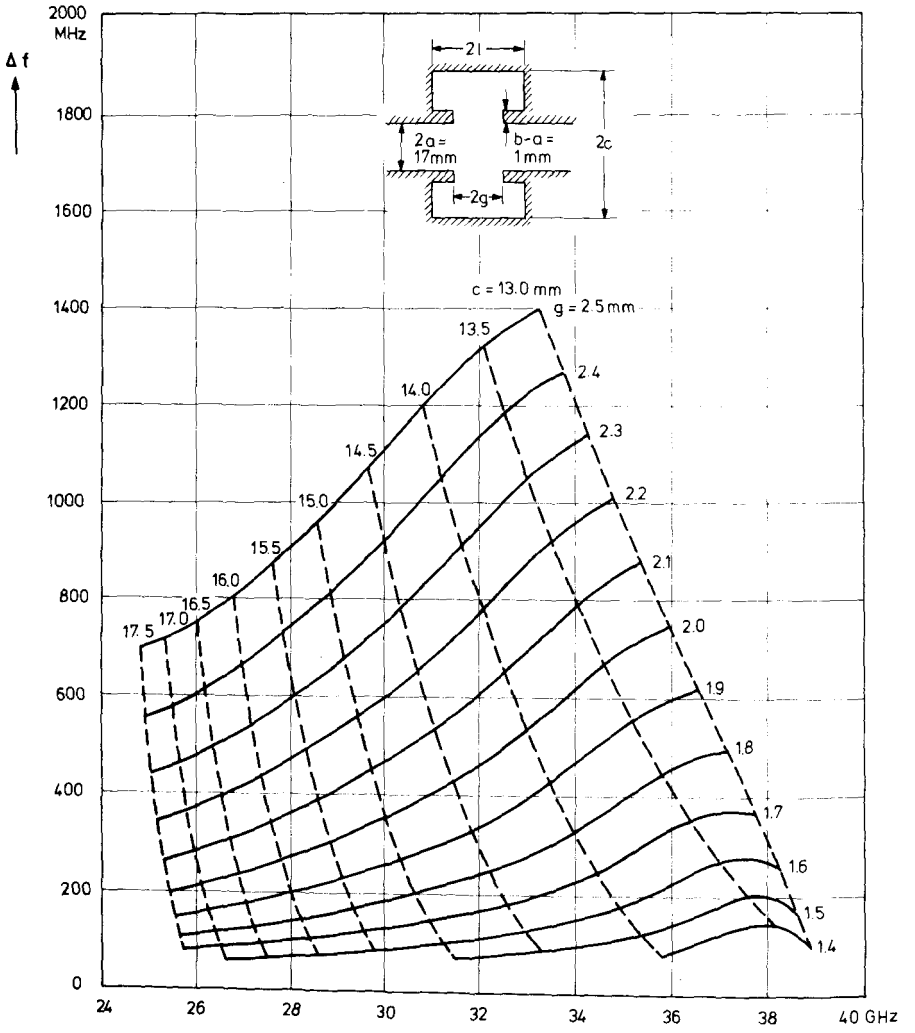

Fig. 8 (c) $\ell = 4.0$ mm.

these requirements can be met. A suitable design yields a sufficiently broad pass-band since the TE_{011}° resonance occurs slightly above the cut-off of the TE_{01}° mode in the circular waveguide. The characteristic parameters f_0, Δf and Δd are plotted in Fig. 9 as a function of the cavity dimensions. As can be seen from the charts, the stop frequency decreases with increasing outer radius, whereas the bandwidth is broadened. This drawback can partly be compensated by an appropriate choise of the waveguide radius as in the case of the TE_{021}° band-stop filter.

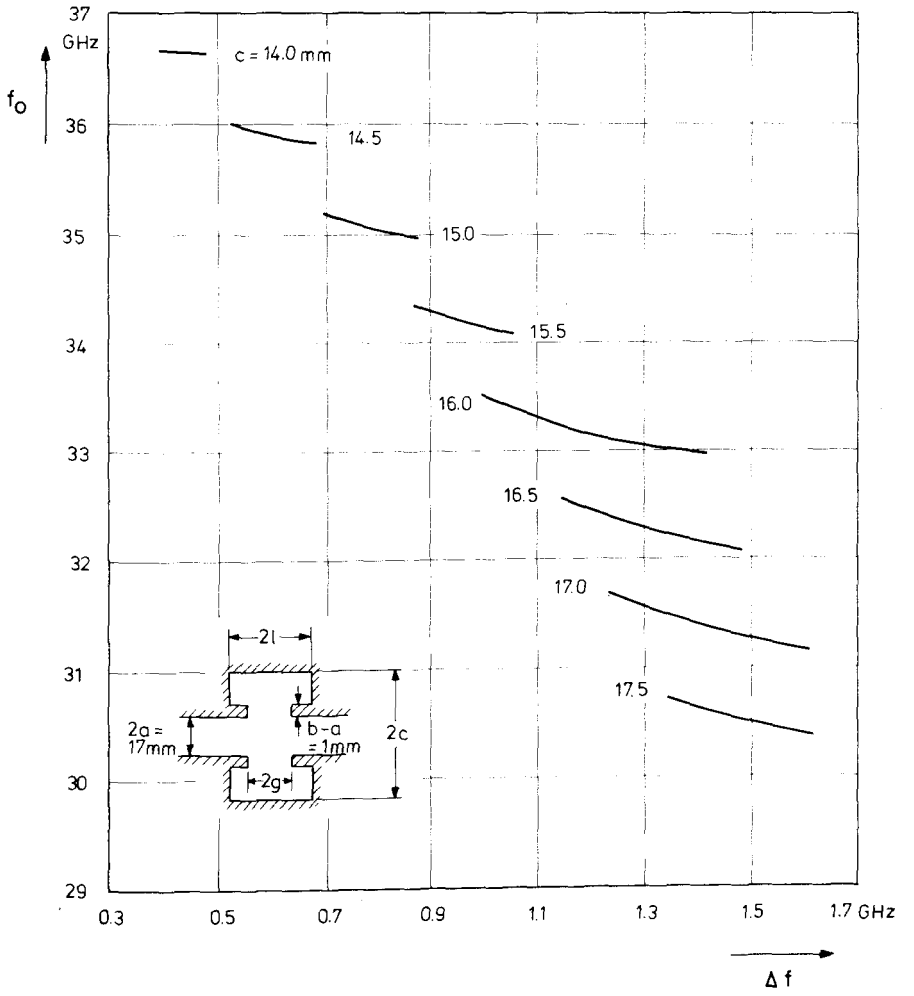

Fig. 9 Design charts for a two-pole TE_{01}° band-stop filter with coaxial cavity (modified TE_{012}°-TE_{013}° resonance)
(a) cavity dimensions,

A simplified equivalent network for this filter is depicted in Fig. 10. It consists of two identical series resonant circuits shunting the line at a distance of $\lambda_{g_0}/4$ from each other. It is worth noting that in contrast to the single-pole filter described by the charts in Fig. 3, the short-circuit planes at resonance are in this case located in front of the symmetry plane. In comparison with two single-pole band-stop filters having comparable frequency characteristics, this filter is superior due to its smaller size and still lower losses.

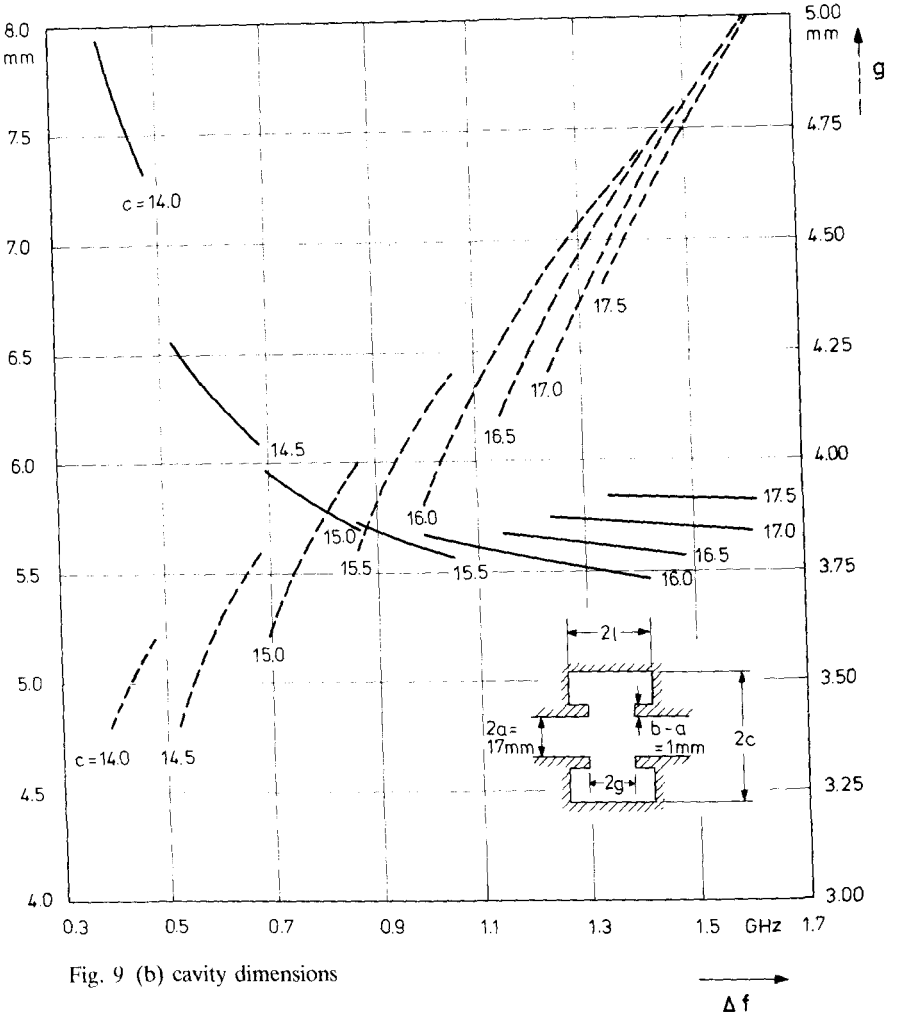

Fig. 9 (b) cavity dimensions

7. Experimental results

In order to check the design and analysis procedures described above, a filter model consisting of two identical, 5 $\lambda_{g_0}/4$-coupled, coaxial TE_{011}° cavities has been constructed and fabricated from brass having a dc conductivity of $\sigma_m = 14 \cdot 10^6/(\Omega m)$. The dimensions are given in Table 1. The two-cavity filter has been designed to yield a BUTTERWORTH type insertion loss response. Theoretical and experimental results concerning the return loss and insertion loss characteristics are plotted in Fig. 11. Good agreement has been obtained between measured and predicted performance. As can be seen from the frequency response curves, the stopped band is almost

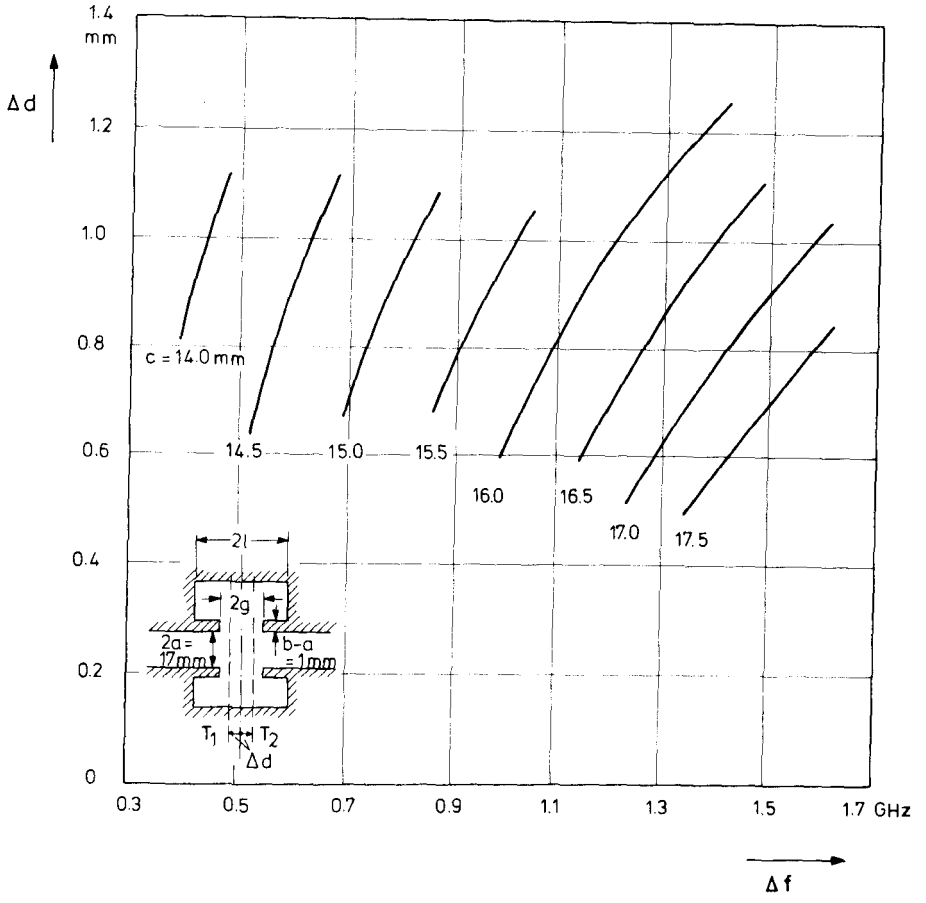

Fig. 9 (c) position of the short-circuit planes at resonance.

completely rejected, a fact which verifies the theoretically derived result that filters utilizing circular electric modes are extremely low-lossy. The ripples occuring in the return loss characteristic are caused by additional reflections of the TE_{01}°-$TE_{10}^{\square}$ mode-transducers used to connect the filter to the measuring set-up constructed in WG22 waveguide.

Following the method for designing cascaded filters, an over-all bandwidth of $\Delta f = 786$ MHz is expected. This value, however, differs from the actual value of about 700 MHz obtained from Fig. 11 by slightly more than 10%. This deviation results from assuming that close to resonance the frequency response of the individual filter can be determined from an equivalent network representation with only one resonant circuit. To overcome this difficulty, a slightly greater 3-dB-bandwidth should be chosen in the design and its actual value can then controlled by the analysis procedure. Merely a few iterations are required to adjust Δf as specified.

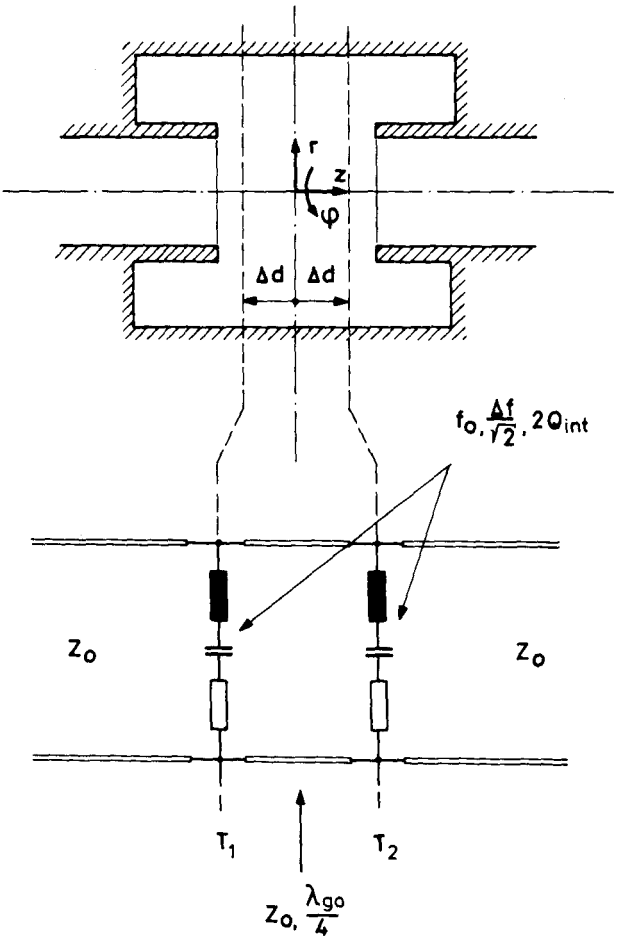

Fig. 10 Equivalent network of a two-pole TE°_{01} band-stop filter valid in the frequency range close to the modified TE°_{012}-TE°_{013} resonance of the coaxial cavity.

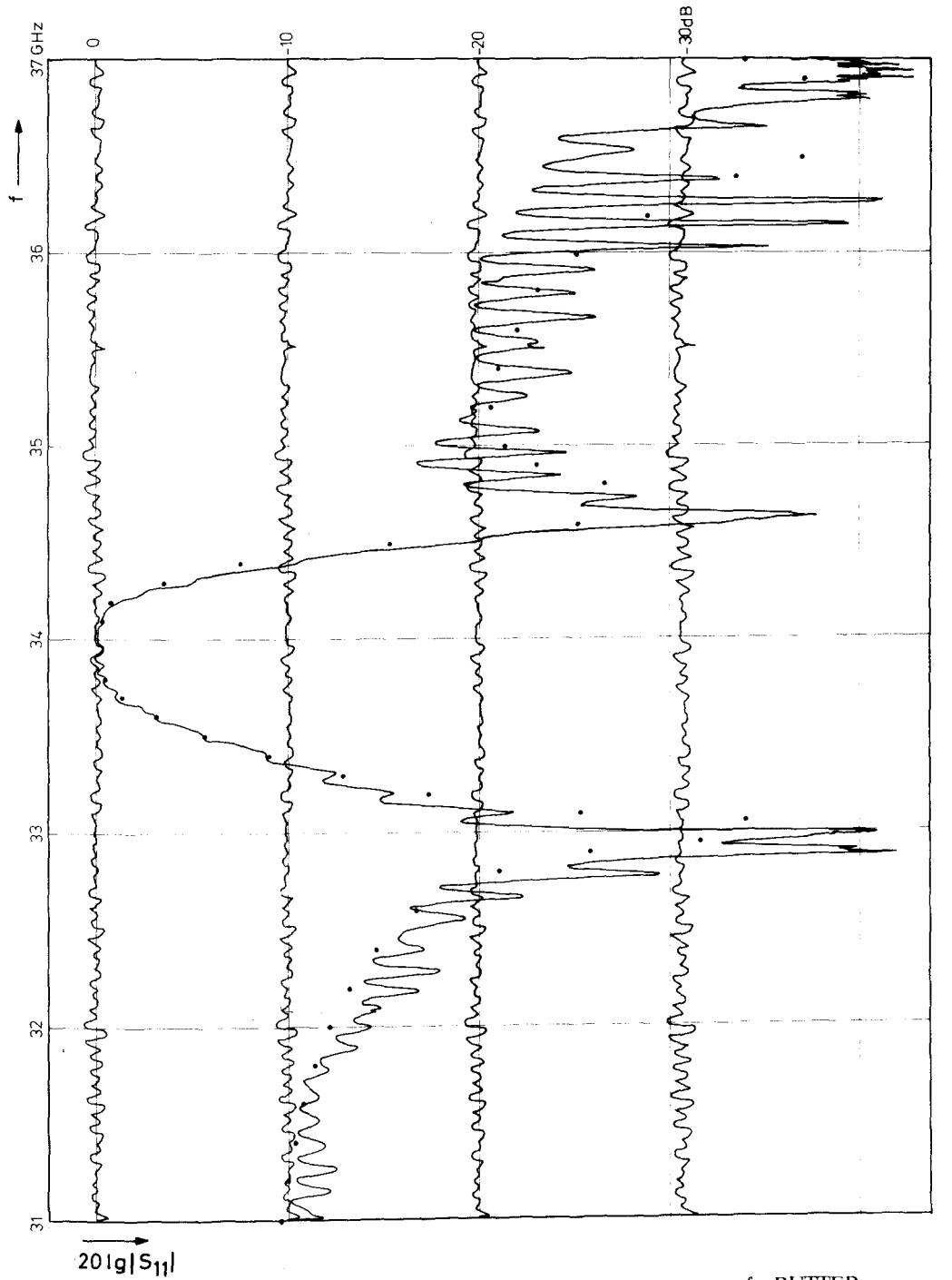

Fig. 11 Comparison of theoretical and experimental frequency response curves of a BUTTERWORTH type TE_{01}° band-stop filter with two identical, single-pole, coaxial cavities utilizing the modified TE_{011}° resonance (a = 8.5 mm, b = 9.5 mm, c = 14.5 mm, g = 2.0 mm, ℓ = 3.0 mm, $\sigma_m = 14 \cdot 10^6/(\Omega m)$, filter separation 5 $\lambda_{g_0}/4$)
... theory ($P^{I} = P^{II} = P^{III} = M^{III} = 10$)
— experiment
(a) return loss

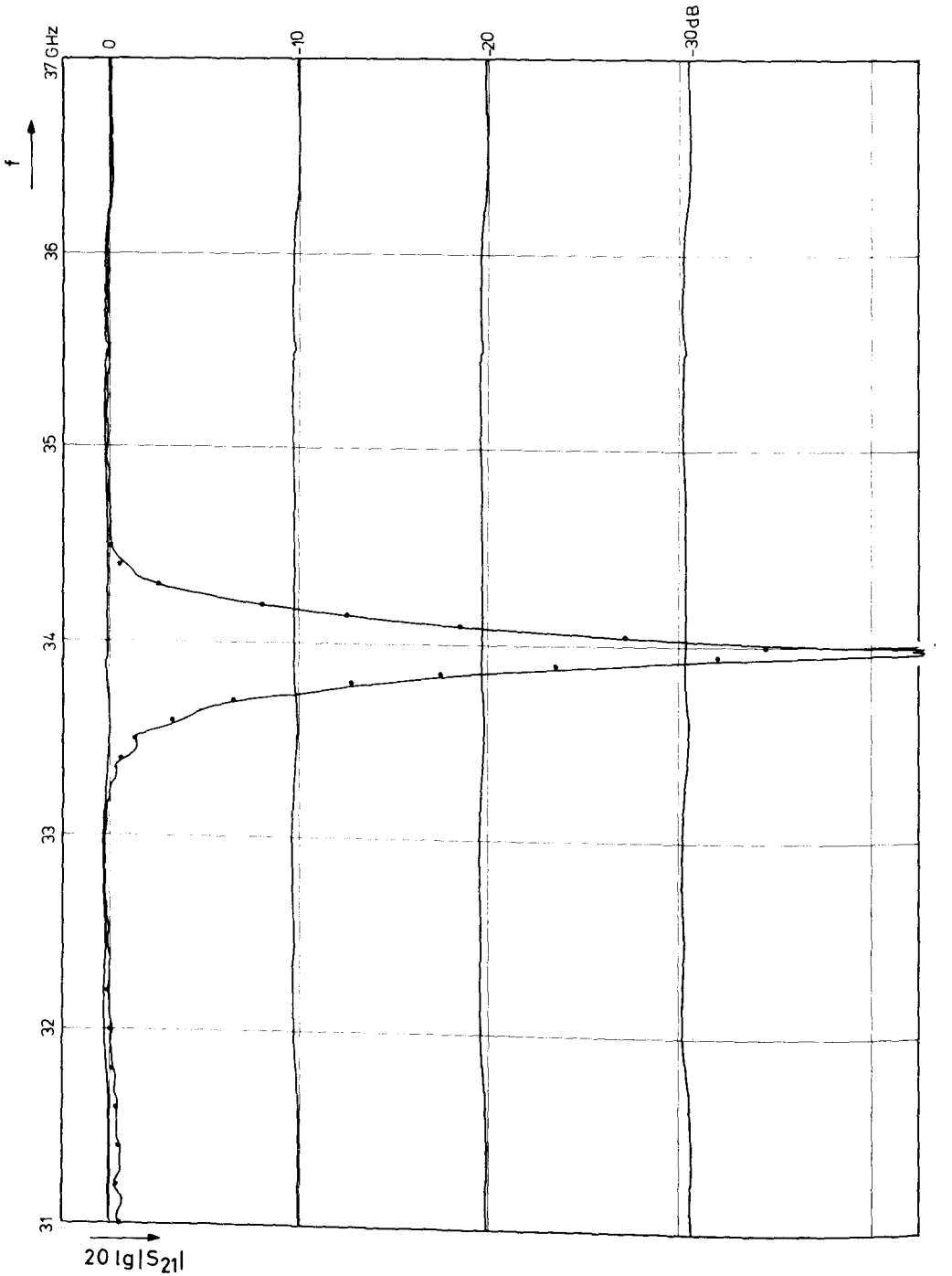

Fig. 11 (b) insertion loss

References

[1] *Marcatili, E. A. J.*, Mode conversion filters, Bell Syst. tech. J. *40* (1961), 149–184.

[2] *Marcatili, E. A. J.*, A channel-dropping filter in the millimeter region using circular electric modes, Transact. Inst. Radio Engrs. MTT-*9* (1961), 176–182.

[3] *Standley, R. D.*, A millimeter wave, two-pole, circular-electric mode, channel-dropping filter structure, Bell Syst. techn. J. *46* (1967), 2261–2276.

[4] *Kühn, E.*, Mikrowellen-Kanalweichen, Dissertation, Technische Universität Braunschweig, 1972.

[5] *Ren, C.-L.*, Design of a channel diplexer for millimeter-wave applications, Transact. Inst. Elect. Electron. Engrs. MTT-*20* (1972), 820–827.

[6] *Unger, H.-G.*, Elektromagnetische Wellen I und II, F. Vieweg & Sohn, Braunschweig 1967.

[7] *Abramovitz, M., and Stegun, I. A.*, Handbook of mathematical functions, Dover Publications, New York 1965.

[8] *Kühn, E.*, A mode-matching method for solving field problems in waveguide and resonator circuits, AEÜ *27* (1973), 511–518.

[9] *Kurokawa, K.*, The expansions of electromagnetic fields in cavities, Transact. Inst. Radio Engrs. MTT-6 (1958), 178–187.

[10] *Matthaei, G. L., Young, L.*, and *Jones, E. M. T.*, Microwave filters, impedance-matching networks, and coupling structures, McGraw-Hill Book Co., New York 1964.